Defence Research Establishment Pacific
Centre de recherches pour la défense pacifique

DREP Technical Memorandum 89-13

(3)

First-Order Bragg SAR Imagery of Kelvin Wakes and Moving Internal Wave Fields

B.A. Hughes

June 1989

Research and Development Branch
Department of National Defence

Canada

Defence Research Establishment Pacific
Centre de recherches pour la défense pacifique

DEFENCE RESEARCH ESTABLISHMENT PACIFIC

CFB Esquimalt, FMO Victoria, B.C. VOS 1BO

DREP Technical Memorandum 89-13

FIRST-ORDER BRAGG SAR IMAGERY OF KELVIN WAKES AND MOVING INTERNAL WAVE FIELDS

by

B. A. Hughes

June 1989

Approved by:

CHIEF

Research and Development Branch
Department of National Defence

Canada

Abstract

Two theoretical investigations are given relating to SAR imaging of perturbed surface waves. The first is an analysis of the effect of a long wavelength corrugation on the SAR image formed by 1st order Bragg scattering from a deterministic sea wave pattern such as a Kelvin wake. A standard SAR processor is assumed. The second is a stochastic treatment of the SAR imagery formed by a 1st order Bragg scattering process from surface waves modulated by the horizontal surface currents of internal waves. Propagational velocities (normalized by the SAR platform velocity) are included to first order. For the Kelvin wake analysis it is shown that the vertical curvature of the corrugating wave can rotate the effective Bragg acceptance angle by up to ~10° for typical wave parameters. For the internal wave analysis, SAR resolutions are given, and in particular it is shown that typical azimuthal velocity components are important in determining the azimuthal resolution dimension of the scene, especially for resolutions of a few metres size.

Résumé

Le texte décrit deux études théoriques sur l'imagerie SAR de vagues de surface perturbées. La première est une analyse de l'effet d'une cannelure de grande longueur d'onde sur l'image SAR formée par la diffusion de Bragg du premier ordre à partir d'un diagramme déterministe des vagues de l'océan, par exemple un sillage Kelvin. On suppose le recours à un processeur SAR standard. La deuxième étude consiste en un traitement stochastique de l'imagerie SAR formée par la diffusion de Bragg du premier ordre de vagues de surface modulées par les courants de surface horizontaux des ondes internes. Les vitesses de propagation (normalisées par la vitesse de la plate-forme SAR) sont données jusqu'au premier ordre. L'analyse de sillage Kelvin permet de démontrer que la courbure verticale de la vague de cannelure peut faire tourner jusqu'à 10° l'angle d'acceptation efficace de Bragg pour des paramètres de vagues typiques. Dans le cas de l'analyse des vagues internes, on précise les valeurs de la résolution SAR, et on constate plus particulièrement que les composantes de vitesse azimutale typiques sont importantes pour déterminer la dimension de résolution azimutale de la scène, en particulier pour les résolutions de l'ordre de quelques mètres.

Table of Contents

List of Tables

List of Figures

1. Introduction

Several studies[1,2,3] have been made of the effect of motion in scene elements on SAR processing. In those studies the nature of the motion has been either random[1], in which case temporal coherence estimates have been given with their effect on the final image, or organized in the form of surface waves[2] but with random phasing relative to the Bragg scatterers. In either case it has been shown that "velocity bunching" takes place, i.e., image misregistrations occur arising from misinterpretations of phase histories due to the combination of platform velocity and scene element velocity. The decorrelation time associated with random motions also serves to increase the effective azimuthal SAR resolution distance[3]. Scene acceleration effects can also be important[2] producing direct changes in resolution.

Two separate problems are discussed in the present paper, SAR imagery of (a) Kelvin wakes, and (b) moving internal wave fields. In both, a spectral description is used for the Bragg scatterers rather than a correlation description. This offers a simplified interpretation based on narrow-band processes. For the Kelvin wakes, a deterministic problem is solved in which the Bragg-scattering field exists (the diverging wake wave-field) in the presence of a long "corrugating" wave (the transverse wake wave-field). The Kelvin wake is assumed to be steady, and so the Bragg-scatterers are phase-locked to the corrugating wave: specifically, both have the same component of phase velocity along the ship's track, namely, the ship's speed. The corrugating field is not particularized to a detailed Kelvin wake structure but is left as an infinite sinusoid. The Bragg scatterers are also left unspecified in detail. The problem is solved in terms of a filter function which, when applied to the Bragg scattering divergent wave field, provides the unsquared complex SAR image. A numerical example is given for conditions pertinent to narrow-V wakes recorded in Dabob Bay, WN[4].

made, and for the present purpose of discussing 1st-order Bragg backscatter, only terms linear in surface wave height will be kept. The ocean will also be treated as being a perfect conductor and only horizontal polarization in the incident radar field will be examined. These last two conditions can be removed but only with some additional algebraic complexity that does not illuminate the central issues of the present problems. The source and receiver will also be modelled as points, but with beam shaping introduced at a later stage.

With these approximations, the scattered field becomes

$$\vec{\psi}(\vec{x},z,t) \simeq \frac{z^2}{4\pi^2c^2} \iint_{-\infty}^{\infty} \frac{\varsigma(\vec{x}',t_R)\vec{S}''(t_s)}{r_1^2 r_2^2}\, d\vec{x}' \qquad (1)$$

where $\vec{\psi}$ is the vector radar field, z is the source-receiver altitude, $\vec{x}(=x,y)$ is a coordinate frame located at and moving with the source-receiver, c is the speed of radar propagation in air, $\vec{S}$ represents the radiated radar field (with units of $\psi\cdot$length), and $\vec{x}'(=x',y')$ is a non-moving coordinate frame fixed to the ambient ocean surface. Furthermore,

$$t_R = t - r_1/c \quad , \qquad (2)$$

$$t_s = t_R - r_2/c - \frac{V}{c^2}(y'-vt) \simeq t - \frac{r_1+r_2}{c} \quad , \qquad (3)$$

$$r_1 = \sqrt{(x-x')^2 + (y+Vt-y')^2 + z^2} \quad , \qquad (4)$$

$$r_2 = \sqrt{x'^2 + (y'-Vt_R)^2 + z^2} \simeq \sqrt{x'^2 + (y'-Vt)^2 + z^2} \quad , \qquad (5)$$

$$\vec{S}''(t_s) = d^2\vec{S}(t_s)/dt_s^2 \quad , \qquad (6)$$

ς = surface waveheight ,

and here V is the aircraft speed oriented along the y-direction (azimuthal), and the centre of the radar beam is oriented along the x-direction (range). The ratio V/c is sufficiently small that the approximate forms of Equations (3) and (5) will be used.

The r_1- and r_2-terms in the denominator of the integrand are sufficiently slowly varying and sufficiently similar that they can be removed from the integral and each set equal to R, the distance from the source-receiver to the centre of the scene element (i.e. pixel). $\vec{S}$ is also narrowband enough in frequency that the approximation

$$\vec{S}'' = -\omega_c^2 \vec{S} \tag{7}$$

can be used with no appreciable loss of accuracy for the present purposes, with ω_c being the central frequency in the radiated radar field.

The vector character of $\vec{\psi}$ and $\vec{S}$ appears only in the radiated fields and it is scalar versions of these that are used in the SAR processing. The conversions take place at the antenna and bring in the beam-shape function. The received voltage is given by

$$v(t) = \int_{-\infty}^{\infty}\iiint \vec{F}_R(x,y,z)\cdot\vec{\psi}(x,y,z,t)\,dxdydz$$

$$= \int_{-\infty}^{\infty}\iiint \vec{F}_R(x,y,z)$$

$$\times \int_{-\infty}^{\infty}\int_{-\infty}^{\infty}\iiint \frac{z_o z_\varsigma(\vec{x}',t_R)S''(t_s)\vec{F}_T(x_s,y_s,z_s)}{r_1^2(x,y,z,t,\vec{x}')r_2^2(x_s,y_s,z_o,t,\vec{x}')}\,d\vec{x}'dx_s dy_s dz_s dxdydz \tag{8}$$

Here, $\vec{F}_T$ is the beam-shaping function for transmission, $\vec{F}_R$ is the beam-shaping function for the receiver, and the vector character of the radiated field is included explicitly in $\vec{F}_T$ with S_1 now merely being the (scalar) time-dependent part. Also, the receiver altitude is now at z rather than being coincident with the transmitter at z_s. Equation (8) can be rewritten as

$$\phi(t) = \int_{-\infty}^{\infty}\int\int \vec{F}_R(x,y,z) \int_{-\infty}^{\infty}\int\int \vec{F}_T(x_s,y_s,z_s)\phi_p(x,y,z;x_s,y_s,z_o;t)dxdydzdx_sdy_sdz_s \quad (9)$$

with

$$\phi_p(t) = \frac{zz_s}{4\pi^2c^2} \int_{-\infty}^{\infty}\int \frac{\varsigma(\vec{x}',t_R)S_1(t_s)}{r_1^2r_2^2}\, \vec{dx}' \quad (10)$$

Because of the far-field condition for the scattering and all the preceding assumptions, Equation (9), with Equation (10) can be simplified into

$$\phi(t) \simeq -\frac{z^2\omega_c^2}{4\pi^2c^2R^4} \int_{-\infty}^{\infty}\int \varsigma(\vec{x}',t_R)S(t_{s_o};x',y'-vt,z)d\vec{x}' \quad (11)$$

where

$$S(t;x,y,z) = S_1(t)B(x,y,z) \quad (12)$$

and B is now the modulus squared of the voltage beam-shape factor. In this form, beam shape is incorporated directly into the scalar S which describes the incident radiation.

The SAR image is formed by matched-filtering $\phi(t)$ with a version of ϕ that would be obtained from a stationary point reflector. The matching is done over the range coordinate i.e., over a t-interval that corresponds to the radar field propagation time from the antenna to the most distant

scatterer to be imaged and back to the antenna. Matching is also done separately over azimuth and for that S and ϕ are modelled as being pulse-trains and the matching summation is performed over a suitable number of contiguous pulses, a number which can represent an aircraft travel distance that is a significant fraction of the azimuthal beamwidth at the sea surface.

For an explicit pulse-train description, Equation (11) becomes

$$\phi_n(\tau) \simeq - \frac{z^2\omega_c^2}{4\pi^2c^2R^4} \iint_{-\infty}^{\infty} \varsigma(\vec{x}, t_n+\tau - \frac{r_{1n}}{c}) S(\tau - \frac{r_{1n}+r_{2n}}{c} ; x', y'-Vt_n, z_o) d\vec{x}' \qquad (13)$$

where τ is time measured from the start of the n^{th} pulse, t_n, and r_{1n} and r_{2n} are ranges at t_n. For most applications τ can be dropped from the time-argument of ς because the radar scattering interval is effectively only a small fraction of a millisecond, a time short enough that the surface height usually does not change appreciably. The same simplification has been made in the spatial argument of S (relating to the beam shape factor in azimuth), because the aircraft travels a very short distance in the radar propagation time and the beam shape is smooth enough that this distance is unimportant.

The point-reflector replica of $\phi(t)$ is obtained by letting ς be a fixed δ-function at location (x_o, y_o). The coordinate y_o is left unspecified for the present but it will eventually be set to zero because the processing will always be considered to be done symmetrically in azimuth about the location of the replica. At this stage also the aircraft speed mismatch can be included by using V_1 rather than V in the replica description, giving

$$\phi_{rep}(\tau) = - \frac{z_o^2\omega_c^2\sigma_o}{4\pi^2c^2R_o^4} S(\tau - \frac{2\sqrt{x_o^2+(y_o-V_1t_n)^2+z_o^2}}{c}) \ . \qquad (14)$$

Here, σ_o is the scattering strength of the point reflector.

For a Gaussian beam shape and Gaussian pulse shape, S takes the form

$$S(t;x,y-Vt_n,z) \simeq e^{-i\omega_c t - i\omega' t^2 - t^2/T_G^2 - (y-Vt_n)^2/Y_G^2} + c.c. \qquad (15)$$

where T_G and Y_G are the Gaussian beamwidth factors in time and azimuth respectively and where c.c. indicates complex conjugate. Here also, frequency modulation is explicitly included by means of the ω'-term, and the range coordinate beam-shape is ignored because it is usually very broad and contributes effectively only to a general shading in the overall image.

In carrying out the matching process, $\phi_n(\tau)$ and $\phi_{rep}(\tau)$ are both demodulated (frequency-shifted to base-band) and only one side of the transform is used (e.g. positive frequencies only). This results in some computational simplicity for digitally formed images although neither step is crucial to image formation. Appropriate range-dependent phase-shifting terms are also incorporated to eliminate extraneous modulation products in the result. The undetected image is given by

$$W(\vec{x}_o) = \sum_n \int_{-\infty}^{\infty} \phi_n(\tau)\phi^*_{rep}(\tau)d\tau \qquad (16)$$

where the ϕ's are now modified as just described and the sum is over N contiguous pulses.

By using Equations (13) and (14), Equation (16) can be written

$$W(\vec{x}_o) \simeq \sum_n \iint_{-\infty}^{\infty} \varsigma(\vec{x}', t_n - \frac{r_{1n}}{c}) \int_{-\infty}^{\infty} (- \frac{z^2\omega_c^2}{4\pi^2c^2R^4} S_D(\tau - \frac{r_{1n}+r_{2n}}{c}; x', y'-Vt_n, z)$$

$$S_D^*(\tau - \frac{2\sqrt{x^2_o+(y_o-V_1t_n)^2+z_o^2}}{c}; x', y'-V_1t_n, z_o)) e^{\frac{2i\omega_c x_o^2}{c\sqrt{x_o^2+z_o^2}}} dx'dy' \qquad (17)$$

where the subscript D on each S indicates demodulation, and positive frequencies only, and the unimportant amplitude scale factor term in ϕ_{rep}, i.e. $z_o^2\omega_c^2\sigma_o/4\pi^2c^2R_o^4$, has been dropped. The purely phase-shifting term $\exp\{2i\omega_c x_o^2/c\sqrt{x_o^2+z_o^2}\}$ is also shown explicitly (although it need not be inside the integral).

For analytical simplicity, the sum on n is approximated as an integral over t_n using the definition

$$t_n = n\Delta \tag{18}$$

where Δ is the time interval between successive radiated pulses. With this transformation, the sum becomes

$$\sum_n \rightarrow \frac{1}{\Delta}\int \ldots dt_n \quad . \tag{19}$$

One further simplifying change can be made, shifting from t_n to the time-argument, t', of ς, i.e.

$$t' = t_n - r_{1n}/c \quad . \tag{20}$$

To the desired degree of accuracy, and using an impulse response formulation, Equation (17) becomes

$$W(\vec{x}_o) = \int_{-\infty}^{\infty}\iiint \varsigma(\vec{x}',t')I(\vec{x}',\vec{x}_o,t')d\vec{x}'dt' \tag{21}$$

where

$$I(\vec{x},\vec{x}_o,t') = \frac{-z^2\omega_c^2}{4\pi^2c^2R^4\Delta}\exp\left\{\frac{2i\omega_c}{c}\frac{x_o^2}{\sqrt{x_o^2+z_o^2}}\right\}\int_{-\infty}^{\infty} S_D(\tau - \frac{r_1+r_2}{c};\ x',y'-Vt' - \frac{Vr_1}{c},z)$$

$$\times\ S_D^*(\tau - \frac{2\sqrt{x_o^2+(y_o-V_1t'-V_1r_1/c)^2+z_o^2}}{c};\ x',y'-V_1t'-\frac{V_1r_1}{c},zo)d\tau \qquad (22)$$

and

$$S_D(t-\epsilon;x,y,z) = e^{\frac{i\epsilon\omega_c}{c} - i\omega'(t-\epsilon)^2 - \frac{(t-\epsilon)^2}{T_G^2} - \frac{y^2}{Y_G^2}} \qquad (23)$$

The r's in Equations (20) and (22) are actually functions of t (see Equations (4) and (5)) but to the required accuracy they may be treated as time-independent, particularly as used in Equation (22). This can be shown by expanding t_R and t about t_n and substituting these expansions into the expressions for r_1 and r_2 and ignoring terms of order V/c that are small.

With all the approximations incorporated, the final expression for I becomes

$$I(\vec{x},\vec{x}_o,t') = -\frac{z^2\omega_c^2}{4\pi^2c^2R^4\Delta}\exp\left[\frac{2i\omega_c}{c}\frac{x_o^2}{\sqrt{x_o^2+z_o^2}} + \frac{i\omega_c}{c}\{r_1+r_2-2r_o\}\right.$$

$$\left. - \left\{\frac{(y'-V_1t')^2+(y'-Vt')^2}{Y_G^2}\right\} - \frac{(r_1+r_2-2r_o)^2}{2c^2T_G^2}\{\omega'^2T_G^4-1\}\right] \qquad (24)$$

where

$$r_1 \simeq \sqrt{x'^2+(y'-Vt')^2+z^2} \quad , \qquad (25)$$

$$r_2 \simeq r_1 \quad , \qquad (26)$$

and

$$r_o \simeq \sqrt{x_o^2+(y_o-V_1t')^2+z_o^2} \quad . \tag{27}$$

This completes the general analysis. Fourier transform descriptions for ς will be used in the following sections but with forms that are specifically relevant for each problem. Also, the r's of Equations (25) to (27) will be binomially expanded about a common position and terms up to and including second order in deviations from this position will be kept. For the Kelvin wake problem, z in Equation (25) will also be allowed to be a function of position in order to describe the effect of the height of the corrugating wave.

3. Kelvin Wakes

The entire wake wave-field including the corrugating portion is reducible to a steady-state by a simple transformation to coordinate axes moving with the source ship. Thus, with $\vec{c}_s$ as the ship's velocity, and with distance measured from the ship being given by $\vec{\eta}$, the following pertain:

$$\vec{\eta} = \vec{x}'-\vec{c}_st' \quad , \tag{28}$$

$$\varsigma(\vec{x}',t') = \varsigma(\vec{\eta}) \quad ,$$

and, from Equation (21)

$$W(\vec{x}_o) = \iint_{-\infty}^{\infty} \varsigma(\vec{\eta}) \int_{-\infty}^{\infty} I(\vec{\eta}+\vec{c}_st',\vec{x}_o,t')dt'd\vec{\eta} \tag{29}$$

The divergent wave-field ς can now be expressed as a two-dimensional Fourier transform,

$$\varsigma(\vec{\eta}) = \iint_{-\infty}^{\infty} p(\vec{k})e^{ik\cdot\vec{\eta}}d\vec{k} \tag{30}$$

so that

$$p(\vec{k}) = \frac{1}{4\pi^2} \iint_{-\infty}^{\infty} \varsigma(\vec{\eta}) e^{-i\vec{k}\cdot\eta} d\vec{\eta} \quad , \qquad (31)$$

and $$W(\vec{x}_o) = \iint_{-\infty}^{\infty} p(\vec{k}) e^{i\vec{k}\cdot\vec{x}_o} \left(\iiint_{-\infty}^{\infty} e^{i\vec{k}\cdot(\eta - x_o)} I(\vec{\eta}+\vec{c}_s t', \vec{x}_o, t') dt' d\vec{\eta} \right) d\vec{k} \qquad (32)$$

The term $e^{i\vec{k}\cdot\vec{x}_o}$ is taken out explicitly in the integrand of this last expression in order that $W(\vec{x}_o)$ may be seen to be simply a filtered version of ς by comparing Equations (32) and (30). The filter function, denoted Q_2, is given by the term in the braces in Equation (32), i.e.,

$$Q_2(\vec{k};\vec{x}_o) = \iiint_{-\infty}^{\infty} e^{i\vec{k}\cdot(\eta - x_o)} I(\vec{\eta}+\vec{c}_s t', \vec{x}_o, t') dt' d\vec{\eta} \qquad (33)$$

and it contains all of the frequency-shaping, phase-shifting and demodulation that the SAR process applies to the ς-field in the Fourier domain. In this steady-state formulation, all of the fluid-dynamically interactive effects of the corrugating field and its currents on the ς-field are contained in $p(\vec{k})$ and need not be expressed explicitly. This simple situation will not hold in the next section which deals with internal wave modulations that have a stochastic nature and there the frequency-shifting effect of the currents in the corrugating field will need to be explicitly incorporated.

To progress further with the Kelvin wake problem it is necessary to return to Equations (24) to (27) and expand the expressions for r_1, r_2 and r_o using the definitions

$$x' = x_o + \mu \quad , \qquad (34)$$

$$y' = Vt' + y'' \quad , \qquad (35)$$

$$y_o = V_1 t' + q'' \quad , \qquad (36)$$

$$z = z_o + \varsigma_T(\vec{\eta}) \quad , \qquad (37)$$

$$R_o = \sqrt{x_o^2 + z_o^2} \quad . \qquad (38)$$

With terms expressed up to and including second order in μ, y", q" and ς_T,

$$r_1 = r_2 = R_o + \frac{\mu x_o + \varsigma_T z_o}{R_o} + \frac{u^2+y''^2+\varsigma_T^2}{2R_o} - \frac{x_o^2\mu^2}{2R_o^3} - \frac{\mu\varsigma_T x_o z_o}{R_o^3}$$

$$- \frac{z_o^2\varsigma_T^2}{2R_o^3} + \ldots . \tag{39}$$

$$r_o = R_o + \frac{q''^2}{2R_o} + \ldots . \tag{40}$$

and, from Equations (24) and (34) to (36)

$$I(\vec{x}', x_o, t') = I(\mu, y'', \vec{x}_o, q'') \tag{41}$$

$$= - \frac{z_o^2\omega_c^2}{4\pi^2\omega_c^2 R_o^4 \Delta} \exp\left[\frac{2i\omega_c}{c}\frac{x_o^2}{R_o} + \frac{i\omega_c}{c}\Phi(\mu, y'', q'') - \frac{y''^2+\{y'' + (V-V_1)/V_1(y_o-q'')\}^2}{Y_G^2}\right.$$

$$\left. - (\mu x_o+\varsigma_T z_o)^2(\omega'^2 T_G^4-1)/2c^2 T_G^2 R_o^2\right] \tag{42}$$

where

$$\Phi(\mu, y'', q'') = r_1+r_2-2r_o$$

$$= 2\frac{\mu x_o+\varsigma_T z_o}{R_o} + \frac{\mu^2 z_o^2}{R_o^3} + \frac{y''^2-q''^2}{R_o} + \frac{\varsigma_T^2 x_o^2}{R_o^3} - 2\frac{\mu\varsigma_T x_o z_o}{R_o^3} \tag{43}$$

and where, by Equations (28), (34) and (36)

$$\mu = \eta_x - x_o + c_{sx}(y_o-q'')/V_1 \quad , \tag{44}$$

$$y'' = \eta_y + (c_{sy}-V)(y_o-q'')/V_1 \quad . \tag{45}$$

Here, η_x and η_y are the components of $\vec{\eta}$, and c_{sx} and c_{sy} are components of $\vec{c}_s$.

The integration in t' in Equation (33) can be performed after converting t' to q" with the use of Equation (36), and the result is

$$Q_2(\vec{k};\vec{x}_o) = \iint_{-\infty}^{\infty} e^{i\vec{k}\cdot(\eta-x_o)} K(\vec{\eta},\vec{x}_o)\, d\vec{\eta} \tag{46}$$

where

$$K(\vec{\eta},\vec{x}_o) = -\frac{z_o^2\omega_c^2}{4\pi^2c^2R_o^4\Delta V_1}\frac{\pi T_G}{\sqrt{2|C_1|}} e^{A_1+B_1^2/4C_1} \tag{47}$$

To obtain this expression, the argument of the exponential in Equation (42) has been written as

$$\arg = A_1 + B_1q" - C_1q"^2 \tag{48}$$

and, by substitution of Equations (44) and (45) into (43) and (42) and subsequent inspection, the coefficients A_1, B_1 and C_1 can be readily obtained. They will not be expressed explicitly here, but, because of the original quadratic-form expansions of r_1, r_2 and r_o, it can be noted that arg itself is at most quadratic in products of $\vec{\eta}$ and q", and so, A_1 is quadratic in $\vec{\eta}$, B_1 is linear in $\vec{\eta}$ and C_1 is constant. The same orders exist for ς_T. A further simplification will also be made to these coefficients, namely that terms quadratic in the small quantities $|\vec{c}_s|/V$ and ς_T/R_o will be ignored. For the usual range of SAR parameters, these quantities are of order 0.1 or less and the ignored quadratic terms are always dominated by linear counterparts.

Without specifying the functional form of ς_T on $\vec{\eta}$, the Fourier transform represented by Equation (46) cannot be carried out. However, insight can be gained into possible effects of ς_T in the resulting image, by examining the special case in which

$$c_{sx} = 0 \tag{49}$$

i.e., the source ship travelling parallel to the SAR aircraft track, and

$$\varsigma_T = \varsigma_o + \eta_y\left(\frac{\partial \varsigma_T}{\partial y}\right)_o + \frac{1}{2}\eta^2_y\left(\frac{\partial^2 \varsigma_T}{\partial y^2}\right)_o \quad . \tag{50}$$

(For simplicity, the processor mismatch is also set equal to zero, i.e., $V=V_1$.)

The surface underlying the Bragg-wave is thus given a tilt and a curvature in the azimuthal direction only. The argument of the exponent in Equation (47) can be put in a quadratic normal form

$$\arg = A - [(\eta_x - x_s)/Res_x]^2 \ln 16 - [(\eta_y - y_s)/Res_y]^2 \ln 16 \tag{51}$$

where Res_x and Res_y represent full-widths at half-maximum and x_s and y_s represent the position in $\vec{\eta}$ at which the maximum occurs. For the case presented by Equations (49) and (50),

$$Res_x = \frac{\frac{cR_o}{\omega' x_o T_G}\sqrt{\ln 4}}{(1+1/\omega'^2 T_G^4)^{1/2}} \tag{52}$$

$$Res_y = \frac{\frac{2cR_o}{\omega_c T_G}\sqrt{\ln 4}}{(1-4(\frac{\omega' T_G}{\omega_c})^2(\frac{x_o}{Y_G})^2 z_o(\frac{\partial^2 \varsigma_T}{\partial y^2})_o)^{1/2}}(1 + \frac{c_{sy}}{V}) \tag{53}$$

The expression for Res_x is unmodified by the presence of ς_T (to this order), but it can be seen that Res_y can be significantly altered by ς_T's curvature. This gives rise to the possibility of brightened spots appearing in a wake image at positions where there is a coincidence of maximum (positive) $\partial^2 \varsigma_T/\partial y^2$, and Bragg scatterers in the diverging wake components. For stronger conclusions the form of ς_T will be specified more fully and numerical evaluations will be performed.

The specific values chosen for numerical treatment pertain to the Canada Centre for Remote Sensing L-band system (originally constructed by the Environmental Research Institute of Michigan) as configured in July 1983 and used in overflights[4] of Dabob Bay, WN. For JOWIP 8/2

$$\omega_c = 2\pi\ (1.185)10^9 \text{ rad/s} \tag{54a}$$
$$\omega' = 2\pi\ (33.3)10^{12} \text{ rad/s} \tag{54b}$$
$$x_o = 3033.5 \text{ m} \tag{54c}$$
$$z_o = 7010.0 \text{ m} \tag{54d}$$
$$y_o = 0 \text{ m} \tag{54e}$$
$$Y_G = 162.1 \text{ m} \tag{54f}$$
$$T_G = 0.951\ 10^{-6} \text{ s} \tag{54g}$$

where the last two values are Gaussian equivalents which result in unperturbed resolution widths of $\sqrt{20}$ m in both directions. For JOWIP 8/2,

$$V = 134 \text{ m/s} \tag{54h}$$
$$c_s = 8 \text{ m/s along a direction } \sim 13^\circ \text{ off azimuth} \tag{54j}$$

and the amplitude of the corrugating wave had a value of

$$\varsigma_o \simeq 0.1 \text{ m} \tag{54k}$$

at a distance of ~2.5 km behind[9] the source ship (USS QUAPAW). For this ship speed, the wavelength of the corrugating transverse wake component is

$$\lambda_s = 41 \text{ m} \tag{54m}$$

calculated from the gravity wave formula $2\pi c_s^2/g$.

The corrugating wavefield ς_T is modelled as a simple sinusoid. This idealization is used because variations in actual ς_T's perpendicular to the wake axis are minimal, particularly near the axis where the L-band Bragg waves are located in the diverging field. Thus,

$$\varsigma_T = \varsigma_o \cos[\frac{2\pi}{\lambda_s}(\eta_x \sin\theta + \eta_y \cos\theta) + \phi] \tag{55}$$

where θ is the angle of the ship's track with respect to the aircraft track (13° for the present example), and ϕ is a parameter that allows the full range of phase of ς_T to be investigated numerically.

In the Fourier definition of Q_2, Equation (46), the $\vec{\eta}$-coordinate system can be rotated through the angle θ so that ς_T becomes a function of only one variable. Integration can be performed along the orthogonal component of the rotated $\vec{\eta}$ system, and since the exponential argument of K is a quadratic form in $\vec{\eta}$, apart from ς_T, it is also a quadratic form in the rotated system, and the integration simply returns a counterpart quadratic form. The remaining integral, along the direction θ must be done numerically.

In the absence of a corrugating perturbation, Q_2 is a general two-dimensional Gaussian form in $\vec{k}$ and it can be described by its maximum height, the wavenumber position at maximum, and the widths along the $\vec{k}$-axes to the half-maximum points. This is illustrated in contour form in Figure 1. If the peak is also rotated, the angle of rotation is necessary to complete the description. In the presence of the perturbation, these parameters change, and the effect of the perturbation can be described fully by the amounts of the changes. Figure 2 shows the changes in form of the half-maximum contour of Q_2 for different phases, i.e. different values of ϕ in Equation (55), along the corrugating wave. Figures 1 and 2 both use the parameters specified in Equations (54a) to (54m) except for Equation (54k). Figure 1 uses ς_o=0 and Figure 2 uses ς_o=0.5 m.

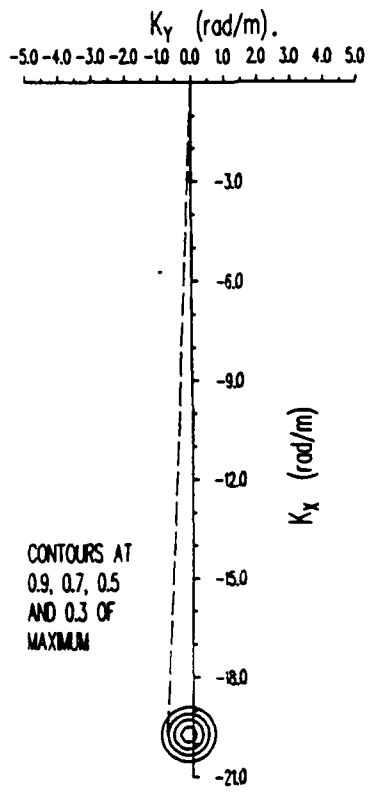

Figure 1. Contours of Q_2 in the absence of a corrugating wave (i.e. ς_o=0) but with the source travelling along θ=13°. The 1st-Bragg wavenumber for this case is (-19.712..,-0.13238..) rad/m. The dotted line indicates the extreme in propagation direction (2.20°) for Q_2 at its half-maximum.

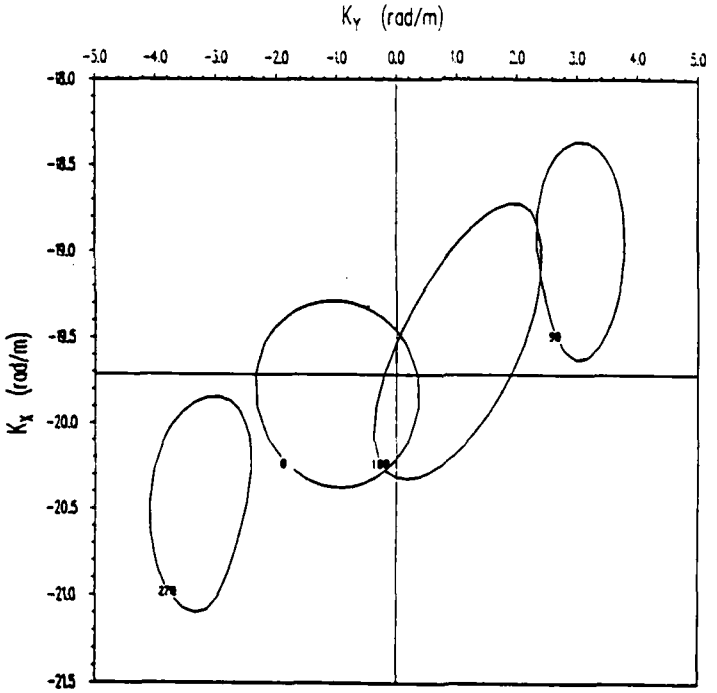

Figure 2. The half-maximum contour of Q_2 for various phases (degrees) along a corrugating wave of amplitude ς_o=0.5 m propagating at θ=13° to the azimuthal direction. Note different scales from Figure 1.

Without a corrugating wave, it can be seen from Figure 1 that surface waves with a wavenumber centered at -19.712..,-0.132 rad/m and within a circular band of width ±0.6240...rad/m are accepted by the processor with a gain of between 1 and 0.5. This bandwidth implies that all waves propagating at an angle within ±1.81° centered at 0.38° off this range direction and with a k_x-value of -19.712 rad/m, are accepted by the processor with a gain reduction of no more than a factor of 2. (The slight offset of the peak from k_y=0 is due to the non-zero value of θ, i.e. the non-zero value of c_{sx}. This range-component of motion in the Bragg scattering wavefield coupled with the aircraft motion and time interval between successive radar pulses results in a slight skewing of the Bragg-wave field in the SAR pattern.)

With a corrugating wave as used in Figure 2, it can be seen that the surface wave wavenumbers accepted by the processor vary over a much more considerable range, allowing waves propagating at up to 11.5° to the range direction to be "seen" (at ϕ=90°), with a gain reduction of no more than a factor of 2 from the peak value. This variation is depicted more fully in Figure 3 where the extreme k_y-value for the half-maximum contour is shown as a function of ϕ for ς_o-values from 0 to 0.5 m. In a similar fashion, extreme k_x-values are shown in Figure 4, and the Q_2-value at its peak is shown in Figure 5, for parameters as in Figure 3.

From Figure 3 it can be seen that the extreme k_y-values are largest for ϕ≈110° (and smallest at 290°). Using the central k_x-value of -19.712 rad/m, the extreme values represent surface waves propagating at angles with respect to the range direction as shown in Figure 6. Here the propagation angles are given as a function of ς_o, and propagation directions that pertain to the center of the processor peak are also given. The displayed data shows strongly linear dependence with ς_o, and very little variation for θ-values over the range θ=0° to 13°.

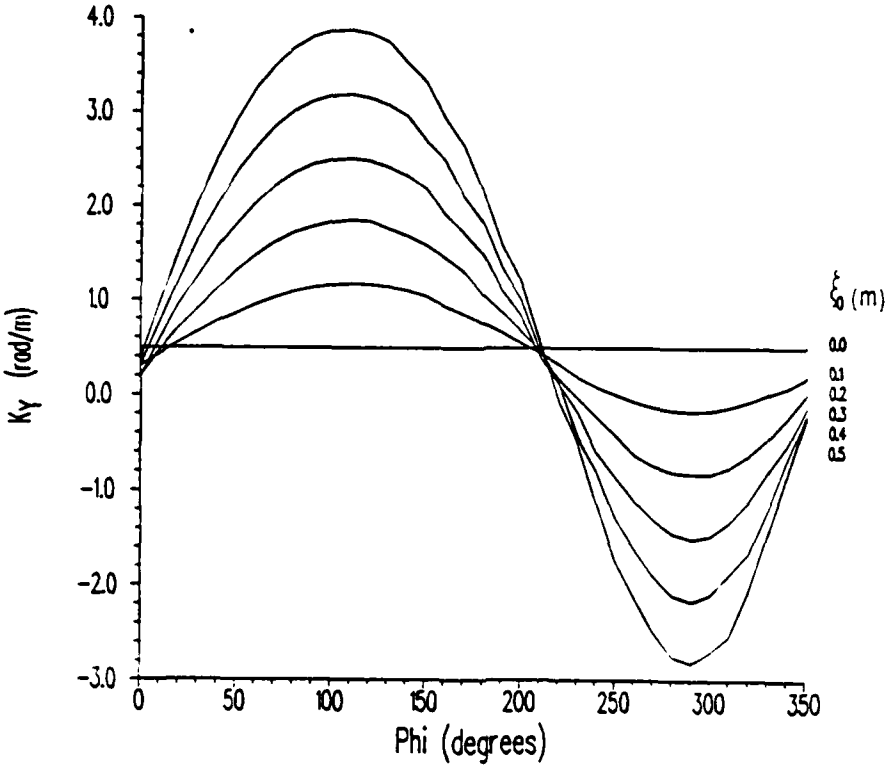

Figure 3. Variations of azimuth wavenumber location for the half-maximum Q_2-contour. Parameter values as given in Equation (54).

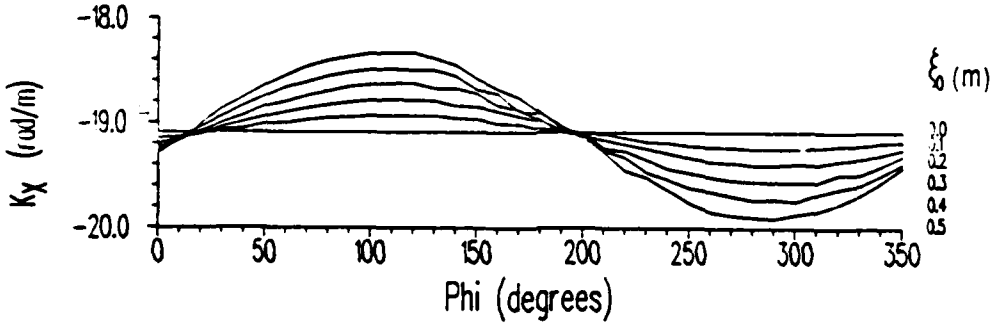

Figure 4. Variations of range wavenumber location for the half-maximum Q_2-contour for the case of Figure 3.

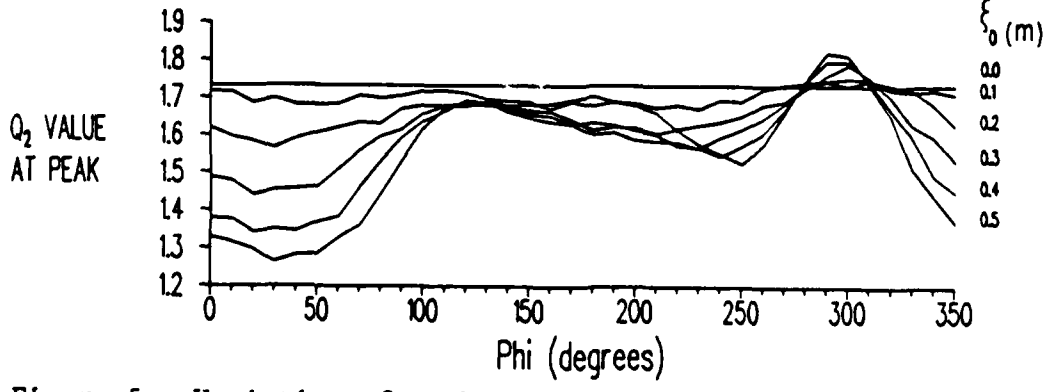

Figure 5. Variation of peak Q_2-value for the case of Figure 3.

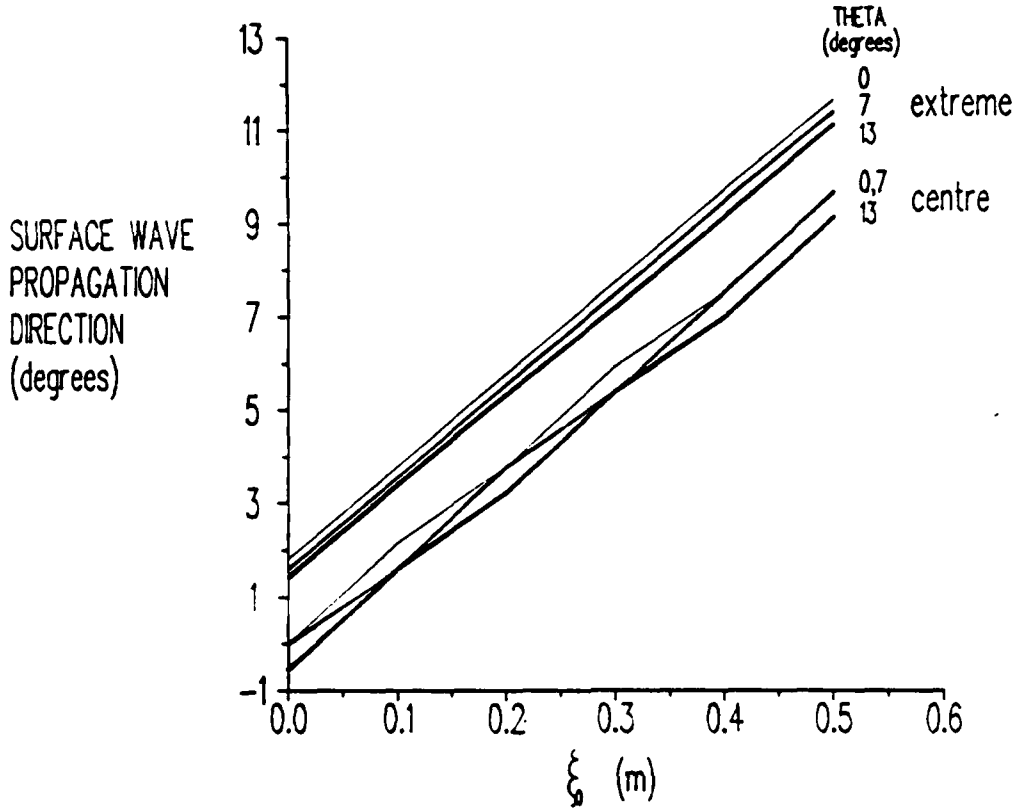

Figure 6. Surface wave propagation direction (as measured from the range coordinate) versus amplitude ς_o of the corrugating wave.

The peak values of Q_2 as given in Figure 5 vary only over the range 3.35 to 4.90 for ς_o=0.5 metres, only 1.6 dB, and so the direct variation of Q_2 is a relatively minor amount. For the Kelvin wake problem, the periodic variation of the filter window in k_y-space is potentially much more significant.

For experimental comparisons, there are three images of clear narrow-V wakes that were taken during the JOWIP measurements, those designated JOWIP 8/2, 8/3 and 9/2. They are shown in Figure 7. From these images the orientation of the most steeply inclined narrow-V arms for each pass have been measured, with respect to the SAR aircraft track, and the values are given in Table 1. Ship track angles as determined from the positioning equipment[10] are also included for each of these runs.

Table 1. Ship Track and Steepest Wake Arm Inclination to SAR Track

SAR Pass	Wake Arm Angle	Ship Track Angle
8/2	18°	13°
8/3	15°	11°
9/2	11°	9°

It can be seen from the Table that the wake arm inclinations are of the same order or are larger than the processor acceptance angles (at half-maximum) for ς_o=0.5 m. However, the variational effects just described will contribute strongly toward enhanced (or decreased) outputs in the SAR image even for these cases.

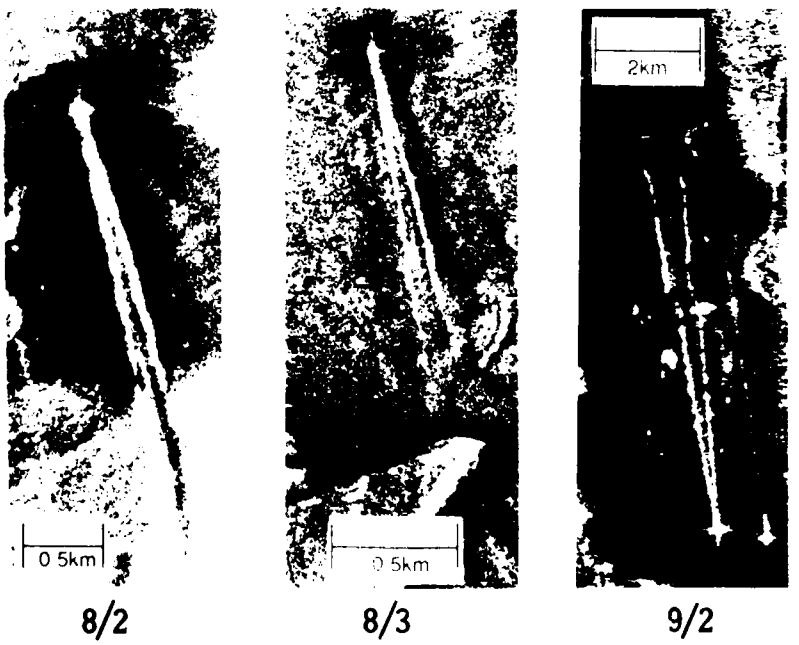

Figure 7. SAR images of narrow-V wakes

4. Internal Waves

In order to determine the effective impulse response function of the SAR system as it pertains to propagating internal wave modulations of surface wave fields, a Fourier description for ς will be used in Equation (21) with modulational features explicitly incorporated. The surface wave field will be specified using a stochastic description rather than a deterministic one as used in the last section. Let ς be described in terms of linear dispersion theory, i.e. frequency σ being a given function of wavenumber $\vec{k}$, but with modulating transform terms A:

$$\varsigma(\vec{x}',t') = \iiint_{-\infty}^{\infty} p_s(\vec{k})A(\vec{k},\sigma_f;\vec{x}',t')\delta(\sigma-\sigma_f-\vec{k}\cdot\vec{U}(\vec{x}',t'))e^{i\vec{k}\cdot\vec{x}'-i\sigma t'}d\vec{k}d\sigma$$

$$+ \iiint_{-\infty}^{\infty} p_s^*(-\vec{k})A^*(-\vec{k},\sigma_f;\vec{x}',t')\delta(\sigma+\sigma_f-\vec{k}\cdot\vec{U}(\vec{x}',t'))e^{i\vec{k}\cdot\vec{x}'-i\sigma t'}d\vec{k}d\sigma \qquad (56)$$

Here $p_s(\vec{k})$ is a wide sense stationary transform, $A(\vec{k},\sigma_f;\vec{x}',t')$ describes the effect of the internal wave modulation on the surface wave field, $\vec{U}$ is the horizontal surface current (assumed to be due to the internal wave field only), and σ_f is the radian frequency of freely propagating surface waves, i.e.

$$\sigma_f = \sqrt{gk+Tk^3} \quad . \qquad (57)$$

In this last equation, g is the acceleration of gravity and T is the surface tension of the air-water interface. In Equation (56), ς is guaranteed to be real by the form of the right-hand side, and the surface wave propagation properties in the presence of the advecting current field $\vec{U}$ are accounted for by the δ-functions.

Equation (56) can be substituted into Equation (21) with the result

$$W(\vec{x}_o) = \int_{-\infty}^{\infty}\int [p_s(\vec{k})\{ \int_{-\infty}^{\infty}\int\int A(\vec{k},\sigma_f;\vec{x}',t')I(\vec{x}',\vec{x}_o,t')e^{i\vec{k}\cdot\vec{x}'-i\sigma_f t'-i\vec{k}\cdot\vec{U}'t'}d\vec{x}'dt'\}$$

$$+ p_s^*(-\vec{k})\{\int_{-\infty}^{\infty}\int\int A^*(-\vec{k},\sigma_f;\vec{x}',t')I(\vec{x}',\vec{x}_o,t')e^{i\vec{k}\cdot\vec{x}'+i\sigma_f t'-i\vec{k}\cdot\vec{U}'t'}d\vec{x}'dt'\}]d\vec{k} \quad (58)$$

and here, $\vec{U}'$ is an abbreviated notation for $\vec{U}(\vec{x}',t')$.

The image $I(\vec{x}_o)$ is defined as

$$I(\vec{x}_o) = |W(\vec{x}_o)|^2 \quad (59)$$

and so the mean image is given by

$$\langle I(\vec{x}_o)\rangle = \langle |W(\vec{x}_o)|^2\rangle \ , \quad (60)$$

i.e.,

$$\langle I(\vec{x}_o)\rangle = \int_{-\infty}^{\infty}\int P_s(\vec{k}) \int\ldots\int_{-\infty}^{\infty} A(\vec{k},\sigma_f;\vec{x}',t')A^*(\vec{k},\sigma_f;\vec{x}",t")I(\vec{x}',\vec{x}_o,t')I^*(\vec{x}",\vec{x}_o,t")$$

$$+ \int_{-\infty}^{\infty}\int P_s^*(-\vec{k}) \int\ldots\int_{-\infty}^{\infty} A(-\vec{k},\sigma_f;\vec{x}",t")A^*(-\vec{k},\sigma_f;\vec{x}',t')I(\vec{x}',\vec{x}_o,t')$$

$$\times I^*(\vec{x}",\vec{x}_o,t")e^{i\vec{k}\cdot(x'-x")+i\sigma_f(t'-t")-i\vec{k}\cdot(U't'-U"t")}d\vec{x}'dt'd\vec{x}"dt"d\vec{k} \quad (61)$$

where $P_s(\vec{k})$ is the power spectrum of the $p_s(\vec{k})$ process, defined by

$$\langle p_s(\vec{k})p_s^*(\vec{k}')\rangle = P_s(\vec{k})\delta(\vec{k}-\vec{k}') \quad (62)$$

In order to proceed further, it is helpful to express A by a Fourier transform and I by a Fourier-like transform:

$$A(\vec{k},\sigma_f;\vec{x}',t') = \iiint_{-\infty}^{\infty} e^{i\vec{K}\cdot\vec{x}'-i\Omega t'}\phi_B(\vec{K},\Omega;\vec{k},\sigma_f)d\vec{K}d\Omega \tag{63}$$

$$Q_2(\vec{K}',\Omega',\vec{K}";\vec{x}_o) = \iiint_{-\infty}^{\infty} I(\vec{x}',\vec{x}_o,t')e^{iK'\cdot\vec{x}'-i\Omega't'-iK"\cdot\vec{U}'t'}d\vec{x}'dt' \tag{64}$$

With these substitutions Equation (61) becomes,

$$\langle I(\vec{x}_o)\rangle = \iint_{-\infty}^{\infty} P_s(\vec{k})\left|\iiint_{-\infty}^{\infty} \phi_B(\vec{K},\Omega;\vec{k},\sigma_f)Q_2(\vec{k}+\vec{K},\sigma_f+\Omega,\vec{k};\vec{x}_o)d\vec{K}d\Omega\right|^2 d\vec{k}$$

$$+ \iint_{-\infty}^{\infty} P_s(-\vec{k})\left|\iiint_{-\infty}^{\infty} \phi_B^*(\vec{K},\Omega;-\vec{k},\sigma_f)Q_2(\vec{k}-\vec{K},-\sigma_f+\Omega,\vec{k};\vec{x}_o)d\vec{K}d\Omega\right|^2 d\vec{k} \tag{65}$$

and at this stage it is expedient to specialize to <u>weak</u> interactions so that

$$A(\vec{k},\sigma_f;\vec{x}',t') = 1 + A_1(\vec{k},\sigma_f;\vec{x}',t') \quad ; \quad A_1 \ll 1 \quad . \tag{66a,b}$$

Therefore,

$$\phi_B = \delta(\vec{K})\delta(\Omega) + \phi_{A1}(\vec{K},\Omega;\vec{k},\sigma_f) \tag{67}$$

and the squared-term in the first integrand in Equation (65) becomes

$$\left|Q_2(\vec{k},\sigma_f,\vec{k};\vec{x}_o) + \iiint_{-\infty}^{\infty} \phi_{A1}(\vec{K},\Omega;\vec{k},\sigma_f)Q_2(\vec{k}+\vec{K},\sigma_f+\Omega,\vec{k};\vec{x}_o)d\vec{K}d\Omega\right|^2$$

Because of Equation (66b) this becomes

$$|Q_2(\vec{k},\sigma_f,\vec{k};x_o)|^2 + Q_2(\vec{k},\sigma_f,\vec{k};\vec{x}_o) \iiint_{-\infty}^{\infty} \phi^*_{A1}(\vec{K},\Omega;\vec{k},\sigma_f)Q^*_2(\vec{k}+\vec{K},\sigma_f+\Omega,\vec{k};\vec{x}_o)d\vec{K}d\Omega$$

$$+ Q^*_2(\vec{k},\sigma_f,\vec{k};\vec{x}_o) \iiint_{-\infty}^{\infty} \phi_{A1}(\vec{K},\Omega;\vec{k},\sigma_f)Q_2(\vec{k}+\vec{K},\sigma_f+\Omega,\vec{k};\vec{x}_o)d\vec{K}d\Omega$$

and the remaining terms are ignorable, being $O(A_1^2)$cf 1. The squared term in the second integrand transforms in a similar manner. With this substituted in Equation (65), the term in $|Q_2|^2$ can be seen to be simply $\langle I(\vec{x}_o)\rangle_s$, i.e. the image that would have existed in the absence of any modulation, and so, the deviation, due only to the modulational effects, is given by

$$\begin{aligned}\langle I(\vec{x}_o)\rangle - \langle I(\vec{x}_o)\rangle_s = &\iint_{-\infty}^{\infty} P_s(\vec{k})\{Q_2(\vec{k},\sigma_f,\vec{k};\vec{x}_o)\\ &\times \iiint_{-\infty}^{\infty} \phi^*_{A1}(\vec{K},\Omega,\vec{k},\sigma_f)Q^*_2(k\vec{+}K,\sigma_f+\Omega,\vec{k};\vec{x}_o)d\vec{K}d\Omega\}d\vec{k}\\ &+ \iint_{-\infty}^{\infty} P_s(-\vec{k})\{Q_2(\vec{k},-\sigma_f,\vec{k};\vec{x}_o)\\ &\times \iiint_{-\infty}^{\infty} \phi_{A1}(\vec{K},\Omega,-\vec{k},\sigma_f)Q^*_2(k\vec{-}K,-\sigma_f+\Omega,\vec{k};\vec{x}_o)d\vec{K}d\Omega\}d\vec{k}\\ &+ c.c. \qquad (68)\end{aligned}$$

The term Q_2 defined in Equation (64) differs only from the corresponding term of Equation (33) by the presence of the phase-shifting component $K''\vec{\cdot}U't'$ due to the internal wave current. However for typical current values, i.e. 1 m/s, and even for large processor integration times, i.e. 10 seconds, the product U't' is equivalent to only a 10-metre shift in position. This is to be compared with a pixel size of 1 to 10 m in range (the range compression is already included in I in Equation (64)) or a

beamwidth of order 100 m in azimuth. For Gaussian beams, I is a Gaussian shape, and so with the $K''\cdot\vec{U}'t'$ term included up to second order in the $\vec{x}',t'$ variables (see equivalent analysis in Section 3, Equations (39) to (43)), Q_2 can be determined explicitly and it also is a Gaussian function in K-space. Because Q_2 is essentially a Fourier transform of a Gaussian function with ~10-m widths (after the t'-integration), it displays widths in K-space of order 2/10 rad/m and these are centered at its Bragg wavenumber, $\vec{k}_B$. Again, using the numerical values of Equations (54a-g), $\vec{k}_B$ is 19.7 rad/m along the range direction and zero along azimuth, and so, the bandwidth of Q_2 in k-space (as used in Equation (68)) is only ~1% of its central value, i.e. extremely narrow.

From the interaction dynamics, it can be determined that ϕ_{A1} is a broad function of $\vec{k}$, and from estimates of surface wave spectra it is known that $P_s(\vec{k})$ is broad and smooth over bandwidths of order 1%. These functions can then be approximated by their values at $\vec{k}_B$ and removed from the k-integration processes in Equation (68) with very little error. For further analysis the integrands are returned to A_1^* and I using Equations (64) and (63), and in the process the $\vec{k}$-integration is done after the dispersive character of the surface waves is incorporated explicitly up to linear terms in $\vec{k}$ by the equation

$$\sigma_f \simeq \sigma_B + (c_{gB}\vec{\cdot}(k-k_B) \quad . \tag{69}$$

The $\vec{k}$-integration returns δ-functions with arguments $\vec{x}'-\vec{x}''\mp\vec{c}_g(t'-t'')-\vec{U}'t'+\vec{U}''t''$, and, in principle these allow one of the $\vec{x}$-integrals to be performed. The result is

$$\langle I(\vec{x}_o)\rangle - \langle I(\vec{x}_o)\rangle_s = 4\pi^2 P_s(\vec{k}_B) \iiint_{-\infty}^{\infty} I^*(\vec{x}_1",\vec{x}_o,t")I(\vec{x}',\vec{x}_o,t')A_1^*(\vec{k}_B,\sigma_B;\vec{x}',t)$$

$$\times e^{-i\{\sigma_B - c_{gB}\vec{\cdot}\vec{k}_B\}(t'-t")} J(\vec{x}_1",\vec{x}')d\vec{x}'dt'dt"$$

$$+ 4\pi^2 P_s^*(-\vec{k}_B) \iiint_{-\infty}^{\infty} I^*(\vec{x}_2",\vec{x}_o,t")I(\vec{x}',\vec{x}_o,t')A_1(-\vec{k}_B,\sigma_B;\vec{x}',t')$$

$$\times e^{i\{\sigma_B - c_{gB}\vec{\cdot}\vec{k}_B\}(t'-t")} J(\vec{x}_2",\vec{x}')d\vec{x}'dt'dt" \qquad (70)$$

with

$$\vec{x}_{1,2}" = \vec{x}' \mp \vec{c}_{gB}(t'-t") - \vec{U}(\vec{x}',t')t' + \vec{U}(\vec{x}_{1,2}",t)"t" \qquad (71)$$

implicitly defining $\vec{x}"_{1,2}$ ($\vec{x}_1"$ for upper sign and $\vec{x}_2"$ for lower sign). In Equation (70), J is the Jacobian allowing the δ-functions to be integrated and it has the form

$$J = (1 + t"\frac{\partial U_x}{\partial x"})(1 + t"\frac{\partial U_y}{\partial y"}) \qquad (72)$$

evaluated at $\vec{x}_1"$ or $\vec{x}_2"$ as appropriate.

The modulation A_1 is usually described in terms of the energy envelope $E(\vec{k},\sigma_f;\vec{x}',t')$ in which case, by defining the autocorrelation function of the ς-process in terms of the Fourier transform of $P_s(\vec{k})E$ and equating that description to the equivalent expression from Equation (58), the following result pertains:

$$|A(\vec{k},\sigma_f;\vec{x}',t')|^2 = (E+E^*)/2 \tag{73}$$

or, in terms of A_1 and an equivalent E_1 defined as E-1,

$$|A|^2 = 1 + A_1+A_1^* + ..$$

$$= 1 + (E_1+E_1^*)/2 \tag{74}$$

and so,

$$A_1 \simeq E_1/2 \tag{75}$$

For usual applications, current strain rates[11] are less than $0(10^{-2}s^{-1})$ and SAR processing times[2] are less than 10 s, thus in Equations (72) and (70), J can be approximated quite well simply as unity. This also simplifies Equation (71) to the explicit form

$$\vec{x}_{1,2}" = \vec{x}' + \vec{c}_{gB}(t'-t")-\vec{U}(\vec{x}',t')(t'-t") \tag{76}$$

The propagational character of the internal waves can also be incorporated explicitly, and here for simplicity, only dispersionless internal waves will be considered. A single transformation can be made from $\vec{x}',t'$ and $\vec{x}",t"$ frames to coordinates moving with the internal wave $\vec{\eta},t'$ and $\vec{\eta}_{1,2},t"$:

$$\vec{x}' = \vec{\eta}+\vec{c}_I t' \tag{77a}$$

$$\vec{x}_{1,2}" = \vec{\eta}_{1,2}+\vec{c}_I t" \tag{77b}$$

where $\vec{c}_I$ is the phase (and group) velocity of the internal waves. With these changes, Equation (70) can be rewritten as follows (note, from Equation (62), P_s is real):

$$\langle I(\vec{x}_o)\rangle - \langle I(\vec{x}_o)\rangle_s = 2\pi^2 P_s(\vec{k}_B) \iint_{-\infty}^{\infty} E_1^*(\vec{k}_B,\sigma_f,\vec{\eta}) \iint_{-\infty}^{\infty} I(\vec{\eta}+\vec{c}_I t',\vec{x}_o,t')$$

$$\times I^*(\vec{\eta}_1+\vec{c}_I t'',\vec{x}_o,t'')e^{-i(\sigma_B-\vec{c}_{gB}\cdot k_B)(t'-t'')}dt'dt''d\vec{\eta}$$

$$+ 2\pi^2 P_s(-\vec{k}_B) \iint_{-\infty}^{\infty} E_1(-\vec{k}_B,\sigma_f,\vec{\eta}) \iint_{-\infty}^{\infty} I(\vec{\eta}+\vec{c}_I t',\vec{x}_o t')$$

$$\times I^*(\vec{\eta}_2+\vec{c}_I t'',\vec{x}_o,t'')e^{i(\sigma_B-c_{gB}\vec{\cdot}k_B)(t'-t'')}dt'dt''d\vec{\eta}$$

$$+ \text{complex conjugate} \qquad (78)$$

With a further definition of the inner double integrals in Equation (78) as impulse response functions $K_{a,b}$, this last form becomes

$$\langle I(\vec{x}_o)\rangle - \langle I(\vec{x}_o)\rangle_s = 2\pi^2 P_s(\vec{k}_B) \iint_{-\infty}^{\infty} E_1(\vec{k}_B,\sigma_f,\vec{\eta})K_a(\vec{\eta},\vec{x}_o)d\vec{\eta}$$

$$+ 2\pi^2 P_s(-\vec{k}_B) \iint_{-\infty}^{\infty} E_1^*(-\vec{k}_B,\sigma_f,\vec{\eta})K_b(\vec{\eta},\vec{x}_o)d\vec{\eta}$$

$$+ \text{complex conjugate} \qquad (79)$$

where

$$K_{a,b}(\vec{\eta},\vec{x}_o) = \iint_{-\infty}^{\infty} I(\vec{\eta}+\vec{c}_I t',\vec{x}_o,t')I^*(\vec{\eta}_{1,2}+\vec{c}_I t'',\vec{x}_o,t'')$$

$$\times e^{\mp i(\sigma_B-c_{gB}\vec{\cdot}k_B)(t't'')}dt'dt'' \qquad (80)$$

with K_a taking the upper sign and $\vec{\eta}_1$, and K_b the lower sign and $\vec{\eta}_2$.

From Equation (79) it can be seen that the modulation in the image is simply a scaled, filtered version of the Bragg scatterer energy density added to a similar scaled filtered version of the anti-Bragg energy density. The kernel functions $K_{a,b}$ represent filters that depend on position $\vec{x}_o$ (and are not just functions of $\vec{\eta}-\vec{x}_o$).

For the Gaussian beam case, I is given by Equation (24), and, using Equations (25) to (27) and after expanding the exponent in I to second order in t' and t", the integrals in Equation (80) can be evaluated. The results can be put into a standard normal form as follows:

$$K_{a,b}(\vec{\eta},\vec{x}_o) = \frac{z^4\omega_c{}^4T_G{}^2Y_G{}^2}{64\pi^2R_o{}^8c^4\Delta^2V_1{}^2}\Gamma_{a,b}\exp[-4\ln 2\{(\frac{\eta_x-x_s}{Res_x})^2 + (\frac{\eta_y-y_{sa,b}}{Res_y})^2\}$$

$$- B_{a,b}(\eta_x-x_s)(\eta_y-y_{sa,b})] \qquad (81)$$

Here, the $Res_{x,y}$-factors are full-width at half-maximum, and the various terms to first order in c_{gB}/V_1, c_I/V_1, U/V_1 and $(V-V_1)/V_1$ are

$$Res_x = \frac{cR_oT_G}{x_o(\omega'^2T_G^4-1)^{1/2}}\sqrt{\ln 2} \qquad (82)$$

$$Res_y = \frac{2cR_o\sqrt{\ln 2}}{Y_G\omega_c(1+c^2R_o{}^2/Y_G{}^4\omega_c{}^2)^{1/2}}$$

$$\times \{1 - \frac{c_{Iy}}{2V_1} + \frac{V-V_1}{2V_1} + i(\frac{c_{Iy}-c_{gBy}-U_y}{V_1})\frac{\omega_cY_G{}^2}{cR_o}\} \qquad (83)$$

$$x_s = x_o - y_oc_{Ix}/V_1 \qquad (84)$$

$$y_{sa} = y_{sb} = y_o + y_o(\frac{V-V_1-c_{Iy}}{V_1}) + x_o\frac{c_{gBx}+U_x}{V_1\{1+c^2R_o{}^2/Y_G{}^4\omega_c{}^2\}}\ , \qquad (85)$$

$$B_a = B_b = \frac{c_{gBx}+U_x-c_{Ix}}{V_1}\left(\frac{2iY_G^2\omega_c x_o^2}{R_o^3 T_G^2 c^3}(1-\omega'^2 T_G^4)\right.$$

$$\left. + \frac{c_{gBx}+U_x}{V_1}\frac{\omega^2 Y_G^2 z_o^2}{c^2 R_o^4} + \frac{c_{Ix}}{V_1}\frac{2x_o^2}{R_o^2 T_G^2 c^2}(1-\omega'^2 T_G^4)\right) \qquad (86)$$

$$\Gamma_a = \Gamma_b = e^{\left(\frac{c_{gBy}+c_{Iy}+U_y}{2V_1}\right) + \frac{i\omega_c Y_G^2}{cR_o}\left(\frac{c_{gBy}-c_{Iy}+U_y}{2V_1}\right) - \frac{V-V_1}{V_1}} \qquad (87)$$

The differences between these equations and those of the previous section (see particularly Equations (75) and (52) are due completely to the product form of Equation (73) and its convolutional nature. Res_x here is less than Res_x in the Kelvin wake description by a factor of about $\sqrt{2}$.

It should be especially noted that the $\vec{\eta}$-behaviour of $K_{a,b}$ is not confined to the explicit η_x, η_y terms appearing on the right-hand side of Equation (81). The terms Res_y, $y_{sa,b}$ and $\Gamma_{a,b}$ also contain $\vec{\eta}$-behaviour through U_x and U_y. The traditional velocity bunching term $x_o U_x/V_1$ appears in Equation (85) and it produces not only the usual misregistrations but it can also produce variations in image intensity if there are variations in U_x with η_y. This can be seen by considering U_x to be linear in η_y in the exponent of Equation (74) thus effectively changing the y-resolution. In symbolic form, and with $c^2R_o^2/Y_G^4\omega_c^2$ ignored compared to 1 (as is typical), and $U'_{xo}=(\partial U_x/\partial y)_o$,

$$U_x \simeq U_{xo}+\eta_y U'_{xo} \qquad (88)$$

$$y_s \simeq y_{so} + \frac{x_o \eta_y U'_{xo}}{V_1} \qquad (89)$$

$$K_{a,b} \simeq \frac{z^4\omega_c^4 T_G^2 Y_G^2}{64\pi^2 R_o^8 c^4 \Delta^2 V_1^2}\Gamma e^{-4\ln 2\left(\frac{\eta_x - x_s}{Res_x}\right)^2 - 4\ln 2\left(\frac{\eta_y[1-x_o U'_{xo}/V_1]-y_{so}}{Res_y}\right)^2}$$

$$\times e^{-B(\eta_x-x_s)(\eta_y[1-\frac{x_o U_o'}{V_1}]-y_{so})} \qquad (90)$$

If E_1 were independent of $\vec{\eta}$, the E_1-terms could be removed from the integrals in Equation (79) and the integrations performed using Equation (90). The result would be

$$\langle I(\vec{x}_o)\rangle - \langle I(\vec{x}_o)\rangle_s = 2\pi^2[P_s(\vec{k}_B)E_1(\vec{k}_B)+P_s(-\vec{k}_B)E_1^*(-\vec{k}_B)]$$

$$\times \frac{z^4\omega_c^4 T_G^2 Y_G^2}{64\pi^2 R_o^8 c^4 \Delta^2 V_1^2} \Gamma \frac{\pi Res_x Res_y}{\sqrt{1 - \frac{Res_x^2 Res_y^2 B^2}{4}}} \frac{1}{1 - \frac{x_o U'_o}{V_1}} \qquad (91)$$

with the scene intensity showing modulations due to the last term on the right even though no mean modulations were present in the original wave field. The same analysis could have been performed on the $\langle I(x_o)\rangle_s$ term showing that it was perturbed by the same right-hand term, and then E_1 could have been set to zero for the uniform wave field condition. Either way the result would be that the gradient of U_x in y produces pseudo-modulations in standard SAR-processed imagery.

For the symmetric processor case, y_o=0 and it can be seen from Equations (82) to (87) that the scene motion and aircraft mismatch affect only Res_y, y_s and Γ, but Res_x and x_s are unaffected to this approximation. For typical parameters (e.g. Equations (54a) to (54m))

$$\frac{\omega_c Y_G^2}{cR_o} \gg 1 \qquad (92)$$

$$\omega' T_G^2 \gg 1 \qquad (93)$$

and so

$$Res_x \simeq \frac{cR_o}{x_o \omega' T_G} \sqrt{\ln 2} \qquad (94)$$

$$Res_y \simeq \frac{2cR_o\sqrt{\ln 2}}{Y_G\omega_c} \frac{1 + \frac{\omega_c^2 Y_G^4}{c^2 R_o^2}\left(\frac{c_{Iy}-c_{gBy}-U_y}{V_1}\right)2}{1 - \frac{c_{Iy}}{2V_1} + \frac{V-V_1}{2V_1} - i\frac{\omega_c Y_G^2}{cR_o}\left(\frac{c_{Iy}-c_{gBy}-U_y}{V_1}\right)} \tag{95}$$

$$B = \frac{c_{gBx}+U_x}{V_1}\frac{\omega^2 Y_G^2 z_o^2}{c^2 R_o^4} - \frac{c_{Ix}}{V_1}\frac{2x_o^2\omega'^2 T_G^2}{R_o^2 c^2}$$

$$-i\frac{c_{gBx}+U_x-c_{Ix}}{V_1}\frac{2Y_G^2\omega_c x_o^2\omega'^2 T_G^2}{R_o^3 c^3} \tag{96}$$

$$x_s = x_o \tag{97}$$

$$y_s = x_o\frac{c_{gBx}+U_x}{V_1} \tag{98}$$

and Γ is unchanged. With Res_y written as in Equation (95), the exponent of $K_{a,b}$ from Equation (81) can be seen to separate quite readily into a real and an imaginary part. The resultant real resolution in y is thus obtained from the exponential of the real part of the $K_{a,b}$ exponent, multiplied by the cosine of the imaginary part. The resolution width occurs when this product equals 1/2. In symbolic form, and with the $K_{a,b}$ exponent defined to be $\phi_r+i\phi_i$, the resolution width is obtained from

$$e^{\phi_r}\cos\phi_1 = 1/2 \quad . \tag{99}$$

By using Equations (90) and (95) at $\eta_x=x_s$ and with some algebraic manipulations, Equation (99) provides the result

$$(Res_y)_{Real} = \sqrt{\frac{\theta(a/b)}{b}}\frac{2cR_o}{Y_G\omega_c}\left(\left(1 - \frac{c_{Iy}}{2V_1} + \frac{V-V_1}{2V_1}\right)2 + \frac{\omega_c^2 Y_G^4}{c^2 R_o^2}\left(\frac{c_{Iy}-c_{gBy}-U_y}{V_1}\right)2\right) \tag{100}$$

where

$$a = \left(1 - \frac{c_{Iy}}{2V_1} + \frac{V-V_1}{2V_1}\right)2 - \frac{\omega_c^2 Y_G^4}{c^2 R_o^2}\left(\frac{c_{Iy}-c_{gBy}-U_y}{V_1}\right)2 \quad , \tag{101}$$

$$b = \frac{2\omega_c Y_G^2}{cR_o}\left|\left(\frac{c_{Iy}-c_{gBy}-U_y}{V_1}\right)\left(1 - \frac{c_{Iy}}{2V_1} + \frac{V-V_1}{2V_1}\right)\right| \tag{102}$$

and $\theta(a/b)$ is defined implicitly by (see Figure 8)

$$\frac{\ln(2\cos\theta)}{\theta} = a/b \tag{103}$$

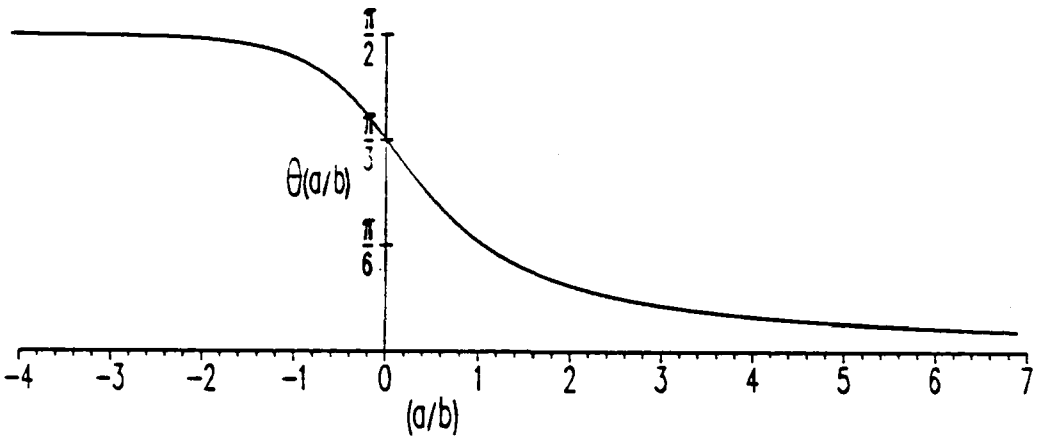

Figure 8. Behaviour of resolution defining function, θ.

For

$$c_{Iy} = c_{gB} = U_y = 0 \tag{104a}$$

and

$$V=V_1 \tag{104b}$$

i.e. no scene motion or aircraft mismatch effects,

$$a/b \to +\infty \tag{105a}$$

$$\theta \to \frac{b\ln 2}{a} \tag{105b}$$

$$a \to 1 \tag{105c}$$

and

$$(Res_y)_{real} \rightarrow \frac{2\sqrt{\ln 2}\ cR_o}{Y_G \omega_c} \quad . \tag{105d}$$

This is the traditional value and it <u>decreases</u> as the width of the processed beam, Y_G, increases.

For c_{Iy}, c_{gB}, U, $\neq 0$ and $Y_G \rightarrow \infty$,

$$a/b \rightarrow -\infty \tag{106a}$$

$$\theta \rightarrow \pi/2 \tag{106b}$$

and

$$(Res_y)_{real} \rightarrow Y_G 2\sqrt{\frac{\pi \omega_c}{cR_o}} \left| \frac{c_{Iy} - c_{gBy} - U_y}{V_1} \right|^{3/2} \quad . \tag{106c}$$

In this limit the resolution <u>increases</u> as the beamwidth Y_G increases and it depends on the azimuthal translation speed of the surface wave Bragg scatterers ($c_{gBy}+U_y$) relative to the azimuthal component of the internal wave phase velocity (c_{Iy}).

For the numerical values of Equations (54a) to (54h), and with

$$c_{Iy} - (c_{gBy}+U_y) = 1 \text{ m/s} \tag{107}$$

the results from Equations (99) to (101) are

$$a/b = 0.4661 \tag{108a}$$

$$\theta = 0.785 \tag{108b}$$

and

$$(Res_y)_{real} \simeq 4.19 \text{ m} \tag{109}$$

This can be compared with 3.16 m obtained from Equation (105d) showing that a not unreasonable amount of azimuthal scene motion can increase the resolution size by a significant amount (33% in this case).

To complete the description of the effect of scene motion it can be seen from Equation (98) that the velocity bunching term should actually be the range-component of the translational velocity of the Bragg-scatterers $c_{gBx} + U_x$ rather than just U_x itself. Furthermore there are small amplitude and phase variations of the K's due to the azimuthal components (and the processor mismatch) as is evident in the Γ's (Equation (87)). The amplitude terms are only of order 1-10% and the phase term is of order 1/2 radian. There is also a small eccentricity of the impulse response peak as shown by the non-zero value of $B_{a,b}$ in Equation (86), and for typical values this is of order 0.40 and dependent solely on the range-components of the scene velocities.

From Equation (59) the covariance of the image can be determined, and using the assumption of Gaussian statistics for the (narrow-band) transform coefficients $p_s(\vec{k})$, the covariance can be shown to be (see Appendix)

$$\mathrm{cov}_I(\vec{\Delta}) = 16\pi^4 P_s^2(\vec{k}_B)\Big[\Big|\iint_{-\infty}^{\infty}\{I_{P1}(\vec{x},\vec{x}_o)I^*_{\beta 1}(\vec{x},\vec{x}_o+\vec{\Delta}) + I_{P2}(\vec{x},\vec{x}_o)I^*_{\beta 2}(\vec{x},\vec{x}_o+\vec{\Delta})\}d\vec{x}\Big|^2$$

$$\times \Big|\iint_{-\infty}^{\infty}\{I_{P1}(\vec{x},\vec{x}_o)I_{P2}(\vec{x},\vec{x}_o+\vec{\Delta}) + I_{P1}(\vec{x},\vec{x}_o+\vec{\Delta})I_{P2}(\vec{x},\vec{x}_o)\}d\vec{x}\Big|^2\Big] \qquad (110)$$

where I_{P1} is the unsquared impulse response function (i.e. whose width defines the pixel size of $w(x_o)$) for positive σ_f and I_{P2} is the same for negative σ_f. It can be seen that if $|\vec{\Delta}|$ is much larger than one pixel dimension the covariance is essentially zero because the products of the I_P's are then zero.

5. Discussion

Kelvin wake narrow-V's in the SAR imagery are considered to be partly due to some randomization and intermittency in the wake structure itself, as is inferred from experimental evidence[12], however, the peculiarities of the SAR processor described above do provide an alternative mechanism for enhancement of local regions of the wake. The fact that these are predicted to occur once per cycle of the transverse wave, and for the enhancements in each of the two arms of the narrow-V to occur at the same transverse wave phase angle, also lends credence to the validity of the effect, because these are in accordance with experimental data. No attempt has been made to model fully the Kelvin wake field, transverse and diverging, because it is known that accurate results for the short wavelength components are very difficult to achieve, requiring complicated source descriptions at the vicinity of the source ship, and also because of the intermittency just referred to. Indeed, the predicted SAR processor variations are not large enough by themselves, but combined with the intermittency and randomization of the direction of the diverging wavefield, they could possibly provide the mechanism underlying the appearance of the brightened V-arms.

The curvature effect examined in Section 3, Equations (50) to (53), can be much larger than traditional velocity bunching effects. The latter are known to produce radar cross section aberrations that are given by[9]

$$|\sigma_{VB}| = z_o \left|\frac{\partial^2 \varsigma_T}{\partial y^2}\right| \frac{c_{sy}}{V_1} \tag{111}$$

where the pattern is considered to be moving in the y-direction as a solid body. The comparable term from the curvature effect is

$$|\sigma_{cur}| = z_o \left|\frac{\partial^2 \varsigma_T}{\partial y^2}\right| 2\left(\frac{\omega' T_G x_o}{\omega_c Y_G}\right)^2 \tag{112}$$

which is obtained by integrating $K(\vec{\eta},\vec{x}_o)$ over all $\vec{\eta}$, as if the Bragg-scatterers covered the entire pixel area uniformly, and using Equations (51), (52) and (53). In Equations (111) and (112) only the perturbations in σ are given. The denominator in Res_y from Equation (53) is also expanded binomially and the first non-unity term kept.

For the numerical values of Equations (54a-j), the relative magnitudes of σ_{VB} and σ_{cur} are 0.06 and 0.5, each of these values coming from the last terms in Equations (111) and (112) respectively. This evaluation is only for a very specific kind of surface (parabolic within the pixel area) and so is only indicative of possibilities. But it does show that curvature effects are not ignorable, a priori.

The perturbation in the SAR processor output due to the curvature of the corrugating wave can be understood from a simple geometrical picture of the radar wave at the sea surface. In the absence of the corrugation, a field of plane radar waves incident on the sea surface at an angle θ_{inc} intersect the surface in a series of straight lines as shown in Figure 9(a). In the presence of a corrugation propagating perpendicularly to the radar waves (in the horizontal), the intersection of the radar waves at the surface also becomes corrugated, with local horizontal wavenumber directions that can be considerably deflected azimuthally from that of the main radar beam, Figure 9(b).

From Figure 10(a), it can be seen that, with z upwards, the radar crest that just intersects the sea surface, as shown, does so at

$$z_i = (x_r - z\tan\theta_{inc})\tan\theta_{inc} \tag{113}$$

If the surface height is specified by a long surface wave with height ς given by

$$\varsigma = \varsigma_o\cos(\vec{k}\cdot\vec{x}+\phi) \tag{114}$$

where ς_o is the wave amplitude, $\vec{k}$ is its wavenumber, $\vec{x}=(x_r,x_a)$ are range and azimuth coordinates, and ϕ is an arbitrary phase angle, then the intersection takes place at

$$z_i = \varsigma \tag{115}$$

which, by Equations (113) and (114) is at

$$x_r - z\tan\theta_{inc} = \frac{\varsigma_o}{\tan\theta_{inc}}\cos(\vec{k}\cdot\vec{x}+\phi) \quad . \tag{116}$$

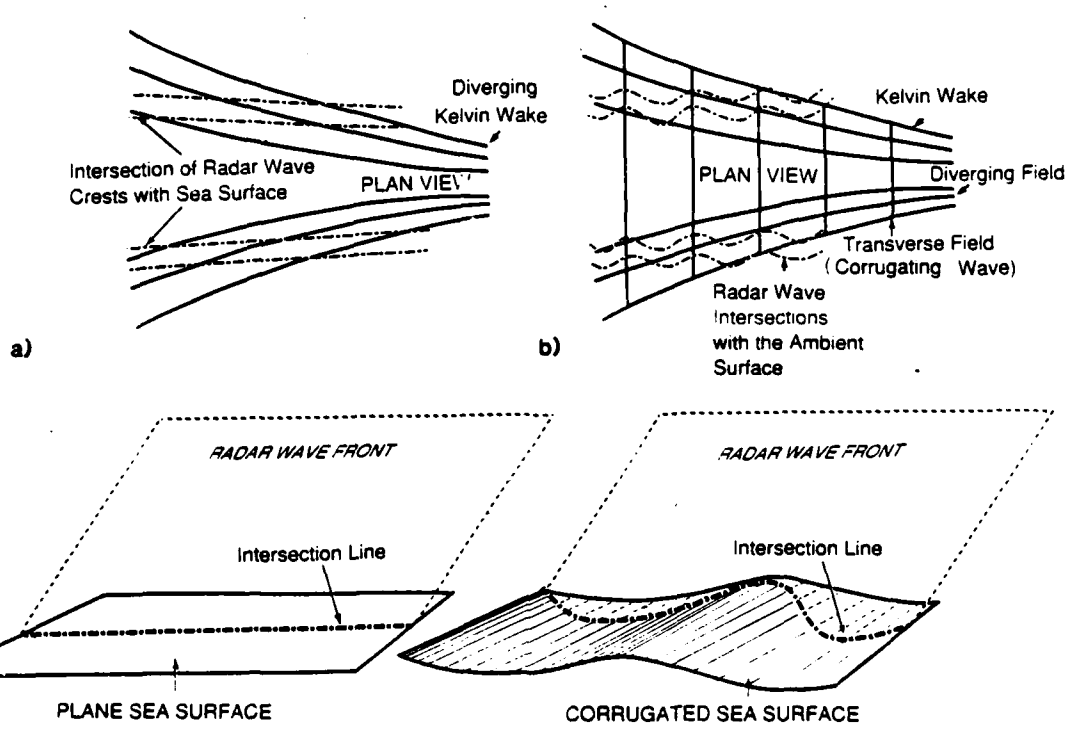

Figure 9. Intersection of the radar beam and the ocean surface (a) non-corrugated, (b) corrugated.

This last can be solved for x_r in terms of x_a (in principle) giving the horizontal shape of the intersection lines. For a corrugation propagating along the azimuth, $\vec{k}\cdot\vec{x} = k_a x_a$ only, and

$$x_r = \frac{\varsigma_o}{\tan\theta_{inc}}\cos(k_a x_a - \phi) + z\tan\theta_{inc} \quad . \tag{117}$$

Typical plan view intersection lines are shown for this case in Figure 10(b).

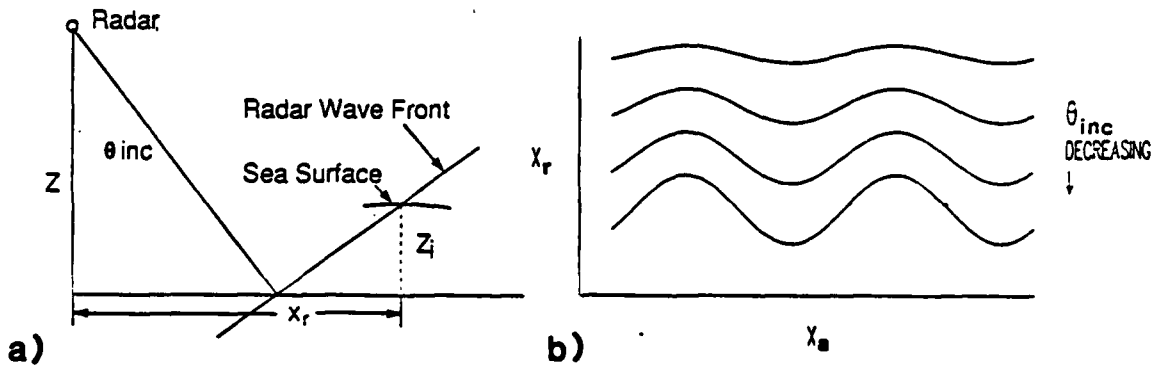

Figure 10. (a) Geometry of intersection (elevation view). (b)Typical horizontal intersection lines for a radar field in the presence of an azimuthally propagating corrugation (plan view).

The slopes of these lines provide estimates of the azimuthal deflection amounts for the effective radar beam in the Bragg scattering process. These deflections allow the scattering to take place from a wider range of horizontal surface wave propagation directions (in the azimuth) than would otherwise be possible. From Equation (117) the slopes are

$$\frac{dx_r}{dx_a} = - \frac{2\pi\varsigma_o}{\lambda_s \tan\theta_{inc}} \sin\left(\frac{2\pi x_a}{\lambda_s} + \phi\right) \tag{118}$$

where λ_s is the wavelength. For the values of Equation (54a-m) but with $\varsigma_o = 0.5$ m,

$$\left|\frac{dx_r}{dx_a}\right| = 0.177 = \tan 10^o \tag{119}$$

This is in accordance with the results of Section 3 where, from Figure 6, the centre of the SAR processor at $\theta=0^\circ$ is aligned with waves propagating at 9.6° (at the maximum deviation).

The internal wave problem has been modelled by Fourier transforms and linear dispersion theory for the surface waves. This essentially resolves the wavefield into sinusoids of uniform height but of random amplitudes and phases (across different realizations). The measure of the coherence of the wave field is contained in its power spectrum and the bandwidths imposed by the radar configuration and the processor. In all cases, the surface waves imaged by the SAR/Bragg-scatter process are coherent over essentially one pixel dimension, regardless of the pixel size (for pixels large compared to a Bragg wavelength). This is apparent for the present model from Equation (110) and it follows directly from the fact that for larger pixels i.e. wider behaviour in I_p, better resolution is obtained in the Fourier domain, i.e. smaller bandwidths pertain and Q_2 is narrower, but these result directly in larger coherence distances. In fact the two are quite simply complementary though the narrow-bandedness of the Fourier description of the power spectrum. For this particular model, broadband coherence distances are irrelevant; only the narrow-band coherences enter the problem. However, if strong non-linearities were present in the surface waves then this simple conclusion would need to be reexamined.

At each pixel location the mean image (Equation (60) rather than Equation (59)), because of its squared nature and all of the SAR processing, is due ultimately to the power in the Bragg waves covering the entire pixel area. If the Bragg wavelengths were much smaller than a pixel dimension so that individual scattering centers could be postulated within the pixel area, then internal correlations between Bragg waves resolved around their

individual centres could be established, and, in keeping with previous work,[1] would likely show uncorrelatedness. In that case the bandwidth of the scattering process would need to be large enough to allow that detailed structure to be faithfully captured in the scattered radar beam, and the SAR processor would need to be wide enough in bandwidth to accept it, otherwise the internal structure within the pixel would be smoothed out and some of the uncorrelatedness would disappear. When the bandwidth of the processor is due to the pixel dimensions, as is the case here (Equations (64) or A(6)), essentially no structure is allowed in the scattering waves within the pixel, and so internal decorrelation distances (or times) cease to be meaningful, and the signal reflected from the pixel becomes uniform across the pixel area, i.e. internally coherent. The power in this coherent signal, as stated earlier, is equal to the average power over the pixel area. This occurs because the Bragg-scattering process is essentially a Fourier transforming process with the SAR processor setting the bandwidths and these in turn setting the pixel size. It should be noted that this concept has been explored previously in connection with surface waves.[2]

The variation of Res_y with Y_G (Equation (99)) is highly significant in attempts to produce very small pixel SAR's to image internal waves. In the example shown in the last section, Equations (106) to (109), a processor that produces a Res_y-value of 3.16 m in the absence of azimuth velocities provides a value of 4.19 m in the presence of 1 m/s components overall (see Equation (107)). If Y_G is increased to 256 m so that the unperturbed pixel size decreases to 2.0 m, the effect of the azimuthal components is to <u>increase</u> this resolution width to 5.4 m, and in fact, further increases in Y_G result in even larger resolution widths. For these parameters an L-band Res_y-value of 2 m is possible but only if R_o is 560 km for Y_G at 162.2 m, and an even larger R_o for Y_G=256 m.

For currents and internal waves moving in the x-direction only, Res_x and Res_y both take on their unperturbed values but the processor peak is rotated by B, and shifted by y_s (Equations (96), (98)). The B-value also

produces some eccentricity, and if the unperturbed processor Res_x- and Res_y-values are equal (as they are for the parameters of Section 3), the eccentricity is of order $(U_x/V_1)^{1/2}$, i.e. ~0.1 and so not of great importance. Here, U_x is the x-component of the surface velocity, and eccentricity is defined as for an ellipse, i.e. $\sqrt{a^2-b^2}/a$ where a and b are the semi-major axes respectively.

6. Conclusion

For the Kelvin wake problem the main conclusion is that large scale surface curvatures can exert a major influence on the processed SAR imagery. For particular cases, as examined in Section 3, the curvatures associated with the corrugating effect of the wake's transverse wave component can readily rotate the processor's Bragg acceptance angle from being bore-sighted with the radar beam to being ~10° fore or aft of the beam. In modelling SAR imaging of Kelvin wakes, particularly for narrow-V effects, this mechanism should be included.

For internal waves, the main conclusion is that azimuthal propagational velocities can strongly affect the resultant azimuthal resolution width of the processor. Also, because of the Fourier description and the use of linear dispersion theory for surface waves, and 1st-order Bragg scattering for the radar reflection, the decorrelation distances are all of order one pixel size. Velocity bunching is shown to be caused by $C_{gBx}+U_x$ rather than just U_x, where C_{gBx} is the range component of the Bragg wave group velocity and U_x is the range-component of the horizontal surface current (vertical velocities have been specifically excluded for this problem). Velocity bunching also produces pseudo-modulation in the imaging if $\partial U_x/\partial y$ is non-zero, where y is the azimuth coordinate.

References

1. Tucker M.J. "The decorrelation time of microwave radar echoes from the sea surface", Int. J. Remote Sens., 6, 1075-1089, 1985.

2. Alpers W.R., D.B. Ross and C.L. Rufenach. "On the Detectability of Ocean Surface Waves by Real and Synthetic Aperture Radar", J. Geophys. Res., 86, 6481-6498, 1981.

3. Raney R.K. "Wave Orbital Velocity, Fade, and SAR Response to Azimuth Waves", IEEE J. Oceanic Engineering, OE-6, 4, 140-146, 1981.

4. Hughes B.A. and T.W. Dawson. "Joint CAN/US Ocean Wave Investigation Project (JOWIP), the Georgia Strait Experiment: An Overview", J. Geophys. Res., 93, C10, 12219-12234, 1988.

5. Alpers W.R. "Theory of Radar Imaging of Internal Waves", Nature, 314, 245-246, 1985.

6. Hughes B.A. "Speckle Noise and Pattern Detection in SAR Imagery of Internal Waves", Technical Memorandum 81-12, Defence Research Establishment Pacific, FMO Victoria, B.C., Canada, VOS 1BO, 1981.

7. Bass F.G. and I.M. Fuks. "Wave Scattering from Statistically Rough Surfaces", translated by C.B. Vesecky and J.F. Vesecky, Pergamon Press, Oxford, 1979.

8. Tsang L., J.A. Kong, and R.T. Shin. "Theory of Microwave Remote Sensing", Wiley-Interscience, 1985.

9. Hammond R.R., R.R. Buntzen and E.E. Floren. "Using Ship Wake Patterns to Evaluate SAR Ocean Wave Imaging Mechanisms", Technical Report 978, Naval Ocean Systems Center, San Diego, CA, 92152-5000, 1985.

10. Hughes B.A. and T.W. Dawson. "DREP Measurements of Surface Ship Wakes in Dabob Bay, WN, July 1983", Report 85-1, Defence Research Establishment Pacific, FMO Victoria, B.C., Canada, VOS 1BO, 1985.

11. Gasparovic R.F., J.R. Apel and E.S. Kasischke. "An Overview of the SAR Internal Wave Experiment", J. Geophys. Res., 93, C10, 12304-12316, 1988.

12. Wyatt D.C. and R.E. Hall. "Analysis of Ship-Generated Surface Waves Using a Method Based Upon the Local Fourier Transform", J. Geophys. Res., 93, C11, 14133-14164, 1988.

Appendix A

Image Covariance

Equation (58) can be written as

$$w(\vec{x}_o) = \iint_{-\infty}^{\infty} p_s(\vec{k}) K_1(\vec{k},\vec{x}_o) d\vec{k} + \iint_{-\infty}^{\infty} p_s^*(\vec{k}) K_2(\vec{k},\vec{x}_o) d\vec{k} \qquad (A1)$$

where K_1 and K_2 represent the triple integrals of the A- and I-functions. The covariance of the image is defined as

$$\mathrm{cov}_I(\vec{\Delta}) = \langle I(\vec{x}_o+\vec{\Delta}) I(\vec{x}_o) \rangle - \langle I(\vec{x}_o+\vec{\Delta}) \rangle \langle I(\vec{x}_o) \rangle \qquad (A2)$$

$$= \langle |w(\vec{x}_o+\vec{\Delta})|^2 |w(\vec{x}_o)|^2 \rangle - \langle |w(\vec{x}_o+\vec{\Delta})|^2 \rangle \langle |w(\vec{x}_o)|^2 \rangle \qquad (A3)$$

The latter form of this equation can be written out in full using Equation (41), and the expectation operator when applied to the quadruple products of the $p_s(\vec{k})$'s can be seen to return double products of the power spectrum $P_s(\vec{k})$, or zero (using Gaussian statistics for $p_s(\vec{k})$). After some lengthy algebraic analysis using Equations (63), (64) and (67), the result for cov_I becomes

$$\mathrm{cov}_I(\vec{\Delta}) = \left| \iint_{-\infty}^{\infty} P_s(\vec{k}) \{ K_1(\vec{k},\vec{x}_o) K_1^*(\vec{k},\vec{x}_o+\vec{\Delta}) + K_2(\vec{k},\vec{x}_o) K_2^*(\vec{k},\vec{x}_o+\vec{\Delta}) \} d\vec{k} \right|^2$$

$$+ \left| \iint_{-\infty}^{\infty} P_s(\vec{k}) \{ K_1(\vec{k},\vec{x}_o) K_2(\vec{k},\vec{x}_o+\vec{\Delta}) + K_1(\vec{k},\vec{x}_o+\vec{\Delta}) K_2(\vec{k},\vec{x}_o) \} d\vec{k} \right|^2, \qquad (A4)$$

and on keeping only the largest terms Equation (A4) becomes,

$$\text{cov}_I(\vec{\Delta}) = \Big|\iint_{-\infty}^{\infty} P_s(\vec{k})\{Q_2(\vec{k},\sigma_f,\vec{k};\vec{x}_o)Q_2^*(\vec{k},\sigma_f,\vec{k};\vec{x}_o+\vec{\Delta})$$

$$+ Q_2(\vec{k},-\sigma_f,\vec{k};\vec{x}_o)Q_2^*(\vec{k},-\sigma_f,\vec{k};\vec{x}_o+\vec{\Delta})\}d\vec{k}\Big|^2$$

$$+ \Big|\iint_{-\infty}^{\infty} P_s(\vec{k})\{Q_2(\vec{k},\sigma_f,\vec{k};\vec{x}_o)Q_2(\vec{k},-\sigma_f,\vec{k};\vec{x}_o+\vec{\Delta})$$

$$+ Q_2(\vec{k},\sigma_f,\vec{k};\vec{x}_o+\vec{\Delta})Q_2(\vec{k},-\sigma_f,\vec{k},\vec{x}_o)\}d\vec{k}\Big|^2 \qquad \text{(A5)}$$

By using the argument given in the main text that Q_2 is a narrow-band function of $\vec{k}$, it is possible to remove the P_s-function from the integrals. Also, the function Q_2 is the Fourier transform of the spatial impulse response function of $w(\vec{x}_o)$, i.e. the smallest resolvable element in the imaged scene (unsquared), and this can be incorporated in the previous equation using the following definition

$$Q_2(\vec{k},\pm\sigma_f,\vec{k},\vec{x}_o) = \iint_{-\infty}^{\infty} e^{i\vec{k}\cdot\vec{x}} I_{p1,2}(\vec{x},\vec{x}_o)d\vec{x} \qquad \text{(A6)}$$

where $+\sigma_f$ selects the impulse response function I_{p1} and $-\sigma_f$ selects I_{p2}. With this definition, and the removal of the $P_s(\vec{k})$'s from the integration, Equation (A5) becomes Equation (110) of the main text.

The impulse response nature of $I_{p1,2}$ can be seen from Equation (64) and the Fourier transform inverse to Equation (A6), which provide

$$I_{p1,2}(\vec{x},\vec{x}_o) = \frac{1}{4\pi^2}\iiint_{-\infty}^{\infty} I(\vec{x}',\vec{x}_o,t') \iint_{-\infty}^{\infty} e^{i\vec{k}\cdot(x'-x)\mp i\sigma_f(\vec{k})t'-i\vec{k}\cdot\vec{U}'t'}d\vec{k}d\vec{x}'dt \qquad \text{(A7)}$$

and, by using Equation (69) the inner double integral can be performed, resulting in a δ-function. By using the Jacobian agrument leading up to Equation (76), the δ-function can be integrated and the final result is

$$I_{p1,2}(\vec{x},\vec{x}_o) = \int_{-\infty}^{\infty} I(\vec{x}\pm\vec{c}_{gB}t'+\vec{U}(\vec{x})t',\vec{x}_o,t')e^{\mp i(\sigma_B - c_{gB}\vec{\cdot}k_B)t'}dt' \qquad (A8)$$

These can be identified directly from Equation (21) as impulse response functions of $w(x_o)$, if the impulse propagates with velocity $\pm\vec{c}_{gB}+\vec{U}$ and displays phase shifts of $\pm(\sigma_B - c_{gB}\vec{\cdot}k_B)t'$, i.e. if

$$\varsigma(\vec{x}',t') = \delta(\vec{x}'-[\vec{x}\pm\vec{c}_{gB}t'+\vec{U}(x)t'])e^{\mp i(\sigma_B - c_{gB}\vec{\cdot}k_B)t'} \qquad (A9)$$

This is precisely in accordance with the linear dispersive nature of the surface waves.

DISTRIBUTION

REPORT: DREP Technical Memorandum 89-13

TITLE: FIRST-ORDER BRAGG SAR IMAGERY OF KELVIN WAKES AND MOVING INTERNAL WAVES

AUTHOR: B. A. Hughes

DATED: June 1989

SECURITY GRADING: UNCLASSIFIED

3 - DSIS
Circulate to:
DRDM
DSP

1 - DREV
1 - DREO
1 - DREA

1 - ORAE Library
1 - D Met Oc
1 - Maritime Tech Library
1 - Bedford Inst. of Oceanography Library
1 - NRC
1 - RRMC Dept of Oceanography
1 - RMC
1 - CRC Library

1 - CDLS (L) CDR
1 - CDLS (W) CDR
1 - DRA Paris

1 - Great Lakes Inst.
University of Toronto

1 - Canada Centre for Inland Waters
Burlington, ON L7R 4A6
Attn: Mr. Mark A. Donelan

10 - DREP

AUSTRALIA

1 - Surveillance Systems Group
Electronics Research Lab
G.P.O. Box 2151
Adelaide, S. Australia 5001
Attn: Dr. D. Cartwright

BRITAIN

Ministry of Defence
1 - DRIC

UNITED STATES

3 - DTIC
1 - Naval Research Laboratory
Washington, D.C. 20375
1 - Environmental Research Inst. of Michigan
P.O. Box 8618
Ann Arbor, Michigan 48107
Attn: Dr. R. Shuchman

3 - Applied Physics Laboratory
Johns Hopkins Road
Laurel, MD 20707
1 - Dr. R. Gasparovic
1 - Dr. R. Gotwols
1 - Dr. D. Thompson

DISTRIBUTION LIST
(Continued)

2 - Naval Ocean Systems Center
San Diego, CA 92152
1 - Dr. R. R. Buntzen
1 - Dr. R. R. Hammond

2 - TRW Inc.
1 Space Park
Redondo Beach, CA 96278
1 - Dr. B. Lake
1 - Dr. K. Kwoh

1 - Dynamics Technology Inc.
1815 N. Lynn St.
Suite 801
Arlington, VA 22209
Attn: Dr. S. Borchardt

1 - Dr. R. S. Winokur
Assoc. Technical Director for
Ocean Science and International Program
Office of Naval Research
Arlington, VA 22217

1 - Defence Advanced Research
Projects Agency,
1400 Wilson Blvd.
Arlington, VA 22209

1 - R & D Associates
P.O. Box 9695
Marina Del Ray, CA 90291
Attn: Dr. D. Holliday

1 - Institute of Geophysics and
Planetary Physics, A-025
Scripps Institution of
Oceanography
La Jolla, CA 92093
Attn: Prof. W. Munk

1 - Dr. Arthur Reed
9106 Warren Street
Silver Spring, MD 20910

1 - Dr. D. Lyzenga
College of Marine Studies
University of Delaware
Newark, DE
19716

DOCUMENT CONTROL DATA

(Security classification of title, body of abstract and indexing annotation must be entered when the overall document is classified)

1. ORIGINATOR (the name and address of the organization preparing the document. Organizations for whom the document was prepared, e.g. Establishment sponsoring a contractor's report, or tasking agency, are entered in section 8.)

Defence Research Establishment Pacific
Forces Mail Office
Victoria, B.C. V0S 1B0

2. SECURITY CLASSIFICATION (overall security classification of the document including special warning terms if applicable)

UNCLASSIFIED

3. TITLE (the complete document title as indicated on the title page. Its classification should be indicated by the appropriate abbreviation (S,C,R or U) in parentheses after the title.)

FIRST-ORDER BRAGG SAR IMAGERY OF KELVIN WAKES AND MOVING INTERNAL WAVES.

4. AUTHORS (Last name, first name, middle initial)

Hughes, Blyth A.

5. DATE OF PUBLICATION (month and year of publication of document)

June 1989

6a. NO. OF PAGES (total containing information. Include Annexes, Appendices, etc.)

47

6b. NO. OF REFS (total cited in document)

12

7. DESCRIPTIVE NOTES (the category of the document, e.g. technical report, technical note or memorandum. If appropriate, enter the type of report, e.g. interim, progress, summary, annual or final. Give the inclusive dates when a specific reporting period is covered.)

TECHNICAL MEMORANDUM

8. SPONSORING ACTIVITY (the name of the department project office or laboratory sponsoring the research and development. Include the address.)

CRAD, DREP

9a. PROJECT OR GRANT NO. (if appropriate, the applicable research and development project or grant number under which the document was written. Please specify whether project or grant)

DRDM-04

9b. CONTRACT NO. (if appropriate, the applicable number under which the document was written)

10a. ORIGINATOR'S DOCUMENT NUMBER (the official document number by which the document is identified by the originating activity. This number must be unique to this document.)

TM 89-13

10b. OTHER DOCUMENT NOS. (Any other numbers which may be assigned this document either by the originator or by the sponsor)

11. DOCUMENT AVAILABILITY (any limitations on further dissemination of the document, other than those imposed by security classification)

- (X) Unlimited distribution
- ( ) Distribution limited to defence departments and defence contractors; further distribution only as approved
- ( ) Distribution limited to defence departments and Canadian defence contractors; further distribution only as approved
- ( ) Distribution limited to government departments and agencies; further distribution only as approved
- ( ) Distribution limited to defence departments; further distribution only as approved
- ( ) Other (please specify):

12. DOCUMENT ANNOUNCEMENT (any limitation to the bibliographic announcement of this document. This will normally correspond to the Document Availability (11). However, where further distribution (beyond the audience specified in 11) is possible, a wider announcement audience may be selected.)

13. ABSTRACT (a brief and factual summary of the document. It may also appear elsewhere in the body of the document itself. It is ghly desirable that the abstract of classified documents be unclassified. Each paragraph of the abstract shall begin with an indication of the security classification of the information in the paragraph (unless the document itself is unclassified) represented as (S), (C), (R), or (U). It is not necessary to include here abstracts in both offical languages unless the text is bilingual).

See page iii.

14. KEYWORDS, DESCRIPTORS or IDENTIFIERS (technically meaningful terms or short phrases that characterize a document and could be helpful in cataloguing the document. They should be selected so that no security classification is required. Identifiers, such as equipment model designation, trade name, military project code name, geographic location may also be included. If possible keywords should be selected from a published thesaurus, e.g. Thesaurus of Engineering and Scientific Terms (TEST) and that thesaurus identified. If it is not possible to select indexing terms which are Unclassified, the classification of each should be indicated as with the title.)

SAR
First Bragg
Kelvin Wakes
Internal Wakes